



Detecting detrital carbonate in shale successions - Relevance for evaluation of depositional setting and sequence stratigraphic interpretation

Juergen Schieber, Xinhe Shao^{*}

Department of Earth and Atmospheric Sciences, Indiana University Bloomington, Bloomington, IN, 47405, USA

ARTICLE INFO

Keywords:

Mudstone microfacies
Sequence stratigraphy
Detrital carbonate
Provenance

ABSTRACT

The Portwood Member of the New Albany Formation is a dolomitic black shale succession that was deposited in the western portion of the Appalachian Basin. Correlative of the Tully Limestone interval found to the northeast in the Appalachian Basin and slightly more than 5 m thick, it nonetheless consists of three erosion-bounded stratal packages that record Late Givetian eustatic sea-level variations. Detailed petrographic study shows that its carbonate interbeds, though readily interpreted as transgressive in nature, are largely detrital, and represent lowstand deposits eroded from the Cincinnati Arch in the west. Petrographical inspection showed abundant silt-sized detrital carbonate within the black shales, as well as a range of other key features, such as mud-dominated composite particles and agglutinated benthic foraminifera, that shed a new and much differentiated light on depositional setting and history of sediment accumulation. Whereas earlier recognized internal erosion surfaces still anchor the sequence stratigraphic framework, reinterpreting carbonate beds as lowstand deposits, and identifying condensed intervals and maximum flooding surfaces via distinct glauconite maxima, supports a reassessment of system tracts that is in agreement with petrographic constraints. Thin section based microfacies analysis identified multiple sedimentary settings, ranging from comparatively shallow (10's of meters, suboxic to dysoxic, tempestites) to very shallow (meters, dysoxic to oxic, wave and current action), and enabled subdivision of the Portwood into a series of upwards shallowing parasequences. This study demonstrates that petrographic due diligence is essential to correctly identify the origin of shale hosted carbonate intervals, and as an added benefit yields a sophisticated understanding of depositional conditions and long-term depositional trends that rivals what is possible for sandstone or carbonate successions.

1. Introduction and geological setting

The Portwood Member of the New Albany Formation was first described by Campbell (1946) who defined it as a basal stratum of the New Albany Shale in eastern Kentucky. The interval is also referred to as *Hypothyridina Zone* due to the presence of a distinctive suite of brachiopods including *Tullypothyridina cenustula*, *Lingulipora venustula*, *Eumetabolotoechia alaura* and *Emmanulla* sp (Campbell, 1946; Brett et al., 2018). Based on fossil data, the Portwood Member is considered time equivalent to the Tully Limestone in the eastern Appalachian Basin (Savage, 1930; Campbell, 1946; Brett et al., 2004). Brett et al. (2018) reviewed the litho- and sequence stratigraphic framework of the Portwood Member on the basis of multiple outcrop sections in east-central Kentucky, found that it is a mappable succession, and established its internal stratigraphy. Study of the Portwood Member is complicated by its extreme lateral variability (no two outcrops are alike; Brett et al.,

2018) and localized soft-sediment deformation associated with tectonic activity (Ettensohn et al., 1988; Brett et al., 2018), impediments that can be overcome through detailed outcrop study and petrography (Brett et al., 2004, 2018).

Lithologically, the Portwood is a carbonate-bearing black shale succession that contains interbedded regionally traceable dolostone layers (Brett et al., 2004). In a conventional sense, carbonate distribution in siliciclastic successions is a property that links to sedimentation rates and indirectly to sea-level change, because in most sedimentation models of siliciclastic-carbonate cycles, carbonate layers are thought to accumulate at high sea level when siliciclastic detritus is trapped in near-shore areas (Van Siclen, 1958; Dolan, 1989; Holland, 1993; Brett et al., 2011). A further assumption is that diagenetic carbonate minerals proliferate in the pore spaces of surface sediments when low sedimentation rates or sediment starvation prevail (Brett, 1995; Wetzel and Allia, 2000; Taylor et al., 2014). Accordingly, laterally extensive

^{*} Corresponding author.

E-mail address: sophiashao0212@yahoo.com (X. Shao).

<https://doi.org/10.1016/j.marpetgeo.2021.105130>

Received 6 January 2021; Received in revised form 5 May 2021; Accepted 10 May 2021

Available online 23 May 2021

0264-8172/© 2021 Elsevier Ltd. All rights reserved.

carbonate beds or horizons with carbonate concretions have traditionally been interpreted as markers for marine flooding surfaces (e.g. Van Wagoner et al., 1990; Taylor et al., 2014; Li and Schieber, 2020). However, as shown in this study, when shale successions accumulate in the vicinity of exposed eroding carbonates, or are onlapping a dissected carbonate platform, the origin of the carbonate component can be more complex. It could for example consist of particles shed from uplifted portions (islands) of an underlying carbonate platform, it could be mixed with siliciclastics if carbonates are exposed in the hinterland of rivers that drain into the basin (Zuffa, 1980), it could be diagenetic pore fills of surficial sediments, and it also could be a mixture of all of these. Sequence stratigraphic interpretations that are guided by the concept that abundant carbonate means high sea level and slow sedimentation can be seriously compromised if clastic carbonate input goes unrecognized.

As demonstrated below, the Portwood Member is an example of a shale unit where the detection of clastic carbonate input is critical for an accurate interpretation of the succession. Through a combination of detailed outcrop sampling, thin section analysis, and SEM analysis, we not only were able to detect the detrital nature of the carbonate component, but also developed a deeper understanding of sedimentary environments and depositional processes, as well as gaining a better appreciation of organic matter (OM) preservation in the succession through recording the stratigraphic variability of carbonate and OM content.

The Portwood was deposited in the western Appalachian Basin, positioned between the Cincinnati Arch in the west and the Acadian Orogen in the east (Fig. 1). During the Middle Devonian, the collision between Laurentia and Avalonian terranes resulted in a high mountain belt (Scotese and McKerrow, 1990) and uplift of the area of Portwood deposition (Ettensohn, 1987). Up to four tectophases that represent continued convergence and successive accretion of Avalonian terranes have been suggested as the underlying cause for large-scale depositional patterns observed in the Appalachian Basin from the Middle Devonian to the Mississippian (Ettensohn, 1985).

Portwood deposition started at the end of the second tectophase and extends into the early parts of the third tectophase of the Acadian Orogeny, marking a major flooding event known as the Taghanic onlap (Johnson, 1970; Ettensohn, 1985, 1994, 2008, 1994; Barnett et al., 1989, 1992, 1992; Brett et al., 2004; Baird and Brett, 2008). The Portwood shows highly variable thickness over short distances, complex internal discordances, and intervals with prominent seismites, collectively suggesting a dynamic interval with active tectonics (Brett et al., 2018). Nonetheless, the fact that in spite of these complications it is possible to trace stratigraphic intervals and discordances from outcrop to outcrop as well as connecting them to Devonian successions elsewhere in the Appalachian Basin indicates the strong influence of eustasy on sedimentation (Brett et al., 2018).

During the Early to Middle Devonian, the study area was located at approximately 30°–35° southern palaeolatitude in the southern subtropics (Witzke and Heckel, 1988; Wilson and Schieber, 2015). The climate in the Cincinnati Arch area is presumed to have been dominantly warm and humid to arid (Scotese, 2001, 2009, 2009; Cocks and Torsvik, 2002).

The unit underlying the Portwood, the Middle Devonian Boyle Formation, is a cherty dolomite in the study area and generally presents an irregular surface with as much as 10 m of local relief due to erosion and karst formation (Brett et al., 2018). Because of this irregular basal contact, the thickness of the Portwood varies dramatically from outcrop to outcrop, and the internal stratigraphy is not readily apparent. Internal sequence-bounding erosion surfaces further complicate correlation, as does the impact of penecontemporaneous tectonics (Brett et al., 2004). The latter is manifest as distinctive intervals showing soft-sediment deformation that have been interpreted as seismites or tsunamites (Barnett and Ettensohn, 2003; Brett et al., 2018). The earthquakes that caused these are thought to be related to reactivation of basement faults

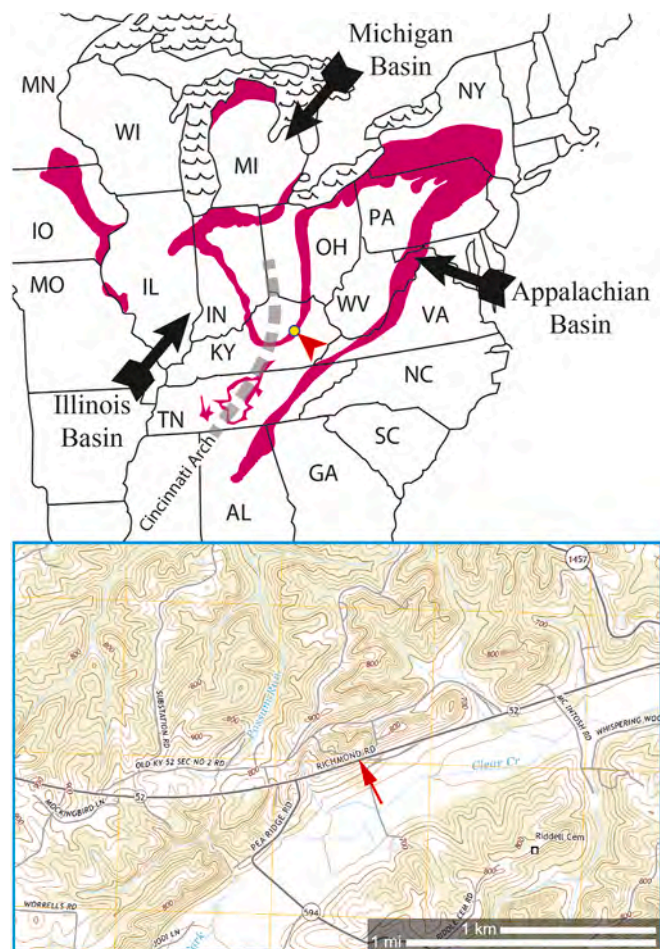


Fig. 1. Location and context of study site. The upper half of the figure shows state boundaries and the outcrop belt of Devonian black shales in magenta. The main depositional basins are marked with black arrows. The outcrop location is marked with a yellow dot and red arrow. The gray dashed line marks the Cincinnati Arch, the dividing line between the Illinois Basin in the west, and the Appalachian Basin in the east. The studied succession is located close to the western margin of the Appalachian Basin. The lower half of the figure shows the location of the outcrop (red arrow) along route 52 between Irvine and Richmond, KY. (For interpretation of the references to color in this figure legend, the reader is referred to the Web version of this article.)

in the Kentucky River fault zone during the second tectophase of the Acadian Orogeny.

Campbell (1946) described three coeval facies in the Portwood Member: the Duffin Dolomite Facies, the Ravenna Shale Facies, and the Harg Shale Facies. The Duffin is a mottled, gray to brownish dolomite breccia; the Ravenna is a dark gray to black fissile shale with lenses of carbonate; and the Harg is composed of greenish, gray or bluish-black argillaceous shale and carbonaceous-calcareous shale. The fissile black shales interfinger with the Harg and the Duffin Bed, and one or two facies may be absent at some locations (Campbell, 1946). In this study (Fig. 2) we adopt the stratigraphic nomenclature of Brett et al. (2018), who re-defined the Portwood Member as consisting of a Lower, Middle, and Upper sub-member, aided by the recognition of regionally traceable dolostone beds. Understanding the origin of these dolostone beds and their stratigraphic significance in the context of vertical stacking of shale facies is the focus of this study.

2. Materials and methods

This study concentrates on an outcrop on Kentucky State Route 52,

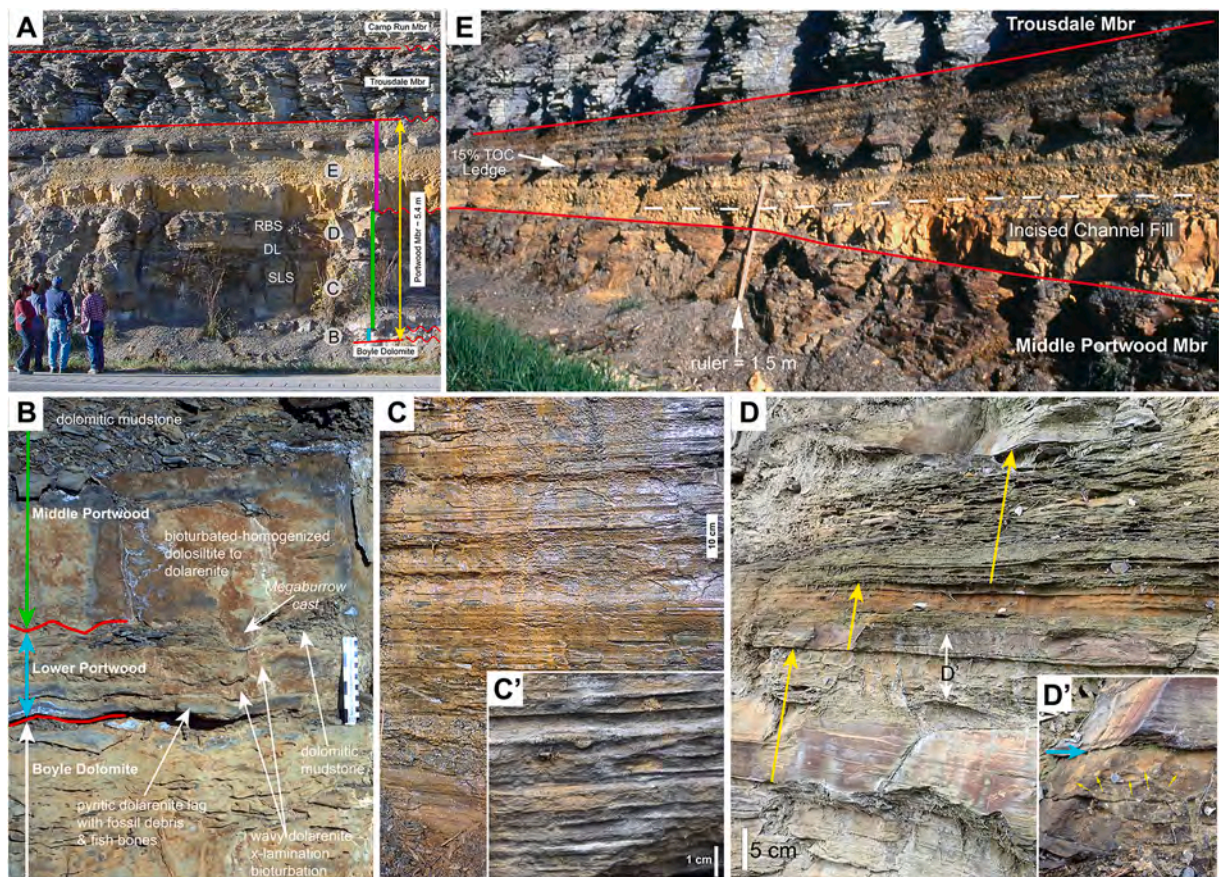


Fig. 2. (A) The Portwood interval in outcrop (yellow double arrow), with its three subdivisions marked by color bars (cyan = Lower Portwood; green = Middle Portwood, purple = Upper Portwood). Under- and overlying stratigraphic units are noted in the figure. Red lines (straight and wavy) are erosion surfaces, SLB = silt laminated black shale, DL = double ledge of dolosiltite beds, RBS = rhythmic black shale (black to gray) cycles. Letters in gray circles correspond to the approximate location of sub-images B, C, D, and E of Fig. 2 (B) Details of the basal contact with the Boyle Dolomite, the Lower Portwood, and the base of the Middle Portwood. (C) Outcrop appearance of the sand-silt laminated carbonaceous shale of the Middle Portwood, inset C' shows details of sand-silt layers. (D) Rhythmic black shale cycles (yellow arrows) in the upper portion of the Middle Portwood, note sharp base of cycles. (D') Closer view of interval marked with double arrow in D. Shows sharp cycle base (cyan arrow) and burrows (yellow arrows) in the top of the underlying cycle. (E) The Upper Portwood with bounding surfaces (red lines) and the left half of an incised channel fill. (For interpretation of the references to color in this figure legend, the reader is referred to the Web version of this article.)

approximately 5 km west of Irvine, Kentucky (Fig. 1), where the Portwood overlies the Boyle Formation, and is capped by the black, fissile Trousdale Member of the New Albany Shale. Exposed in a deeply excavated road cut, the shales are black and appear unoxidized beneath a mm-thick buff-colored weathering rind (Fig. 2). In thin section pyrite framboids and marcasite grains show no sign of alteration. A steep exposure surface was described at cm-to dm-scale. Rock samples were taken approximately every 10 cm vertically, or where lithologic change was noted. All samples were coated with a thin layer of epoxy after return to the laboratory, and then slabbled with a saw and polished with 60–800 grit sandpaper, to aid detailed observation of small-scale sedimentary structures. Thirty-six polished thin sections were prepared from selected samples, and examined with a petrographic microscope (Zeiss PhotoIII) and a FEI Quanta 400 scanning electronic microscope (SEM) to collect information about composition and textural characteristics. The SEM was operated in low vacuum mode to avoid the need for conductive coating of samples, an approach that gives the added benefit of charge contrast for imaging in secondary electron mode. SEM based energy dispersive X-ray spectroscopy (EDS) was used to determine elemental composition of particles. Degree of bioturbation was assessed using a bioturbation index (BI) following suggestions by Lazar et al. (2015a, b). Overview images were obtained by scanning rock slabs and thin sections, and each image was processed in Adobe Photoshop® to enhance subtle sedimentary features.

Powder samples of the Portwood were drilled from the above-

mentioned outcrop surface at a 5 cm vertical spacing. Where surfaces suitable for drilling were not available, small fresh rock pieces were taken back to the laboratory and crushed into powder with mortar and pestle. Approximately 100 mg of organic-rich sample material or ~300 mg of organic-lean sample material (more material needed to be in optimal range of detector) were subjected to acid treatment, using 10% hydrochloric acid (HCl) solution (10% v/v) overnight to dissolve carbonate minerals. Following this, samples were centrifuged and rinsed three times with deionized water to remove remaining HCl and dissolved Ca and Mg ions. After the third wash, samples were placed in a freeze dryer overnight to remove moisture. In this study, mass loss through acid treatment is considered to equal the carbonate mineral content of these rocks (reported as “Carbonate” in Fig. 3). The total organic carbon content (TOC) was analyzed with an ELTRA CS-2000 carbon/sulfur analyzer.

3. Description of the stratigraphic section

The studied exposure, located 5 km due west of Irvine, KY, extends for about 150 m along state highway 52 (Fig. 1). It forms a near vertical cliff (Fig. 2A) at the base of a large road cut that extends to the top of the Devonian, and has been described at various levels of detail by multiple authors (Kepferle and Roen, 1981; Schieber and Lazar, 2004; Brett et al., 2018). The thickness of the Portwood, approximately 5.4 m where measured, varies somewhat along outcrop due to multiple erosion

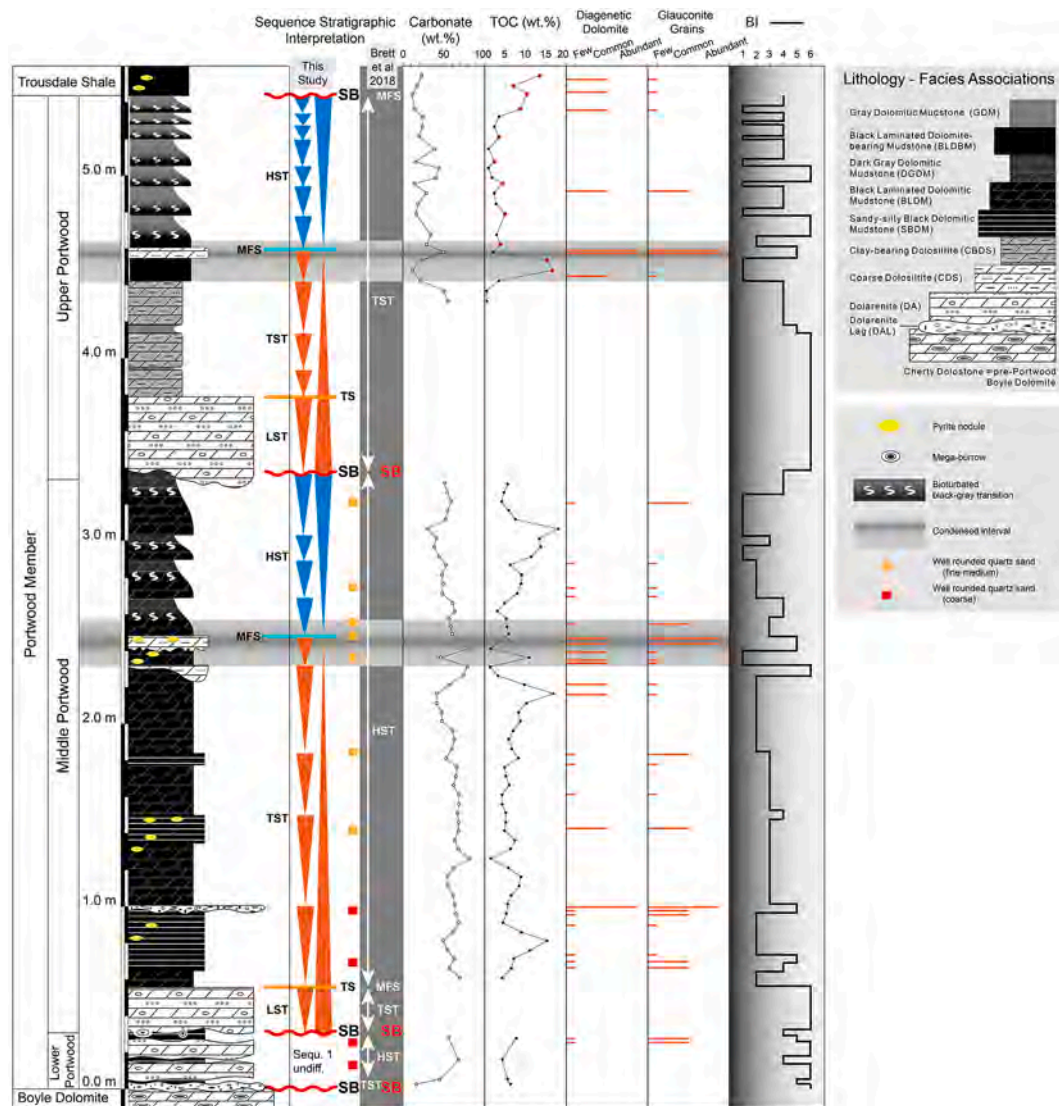


Fig. 3. Detailed stratigraphic section of the Portwood Member, showing major subdivisions, distribution of facies associations (FAs), carbonate and TOC content, glauconite and diagenetic carbonate cement, rounded quartz sand grains, bioturbation intensity (BI) and sequence stratigraphic interpretation. The left-right gray scale gradient in the BI column is intended to show the pervasive nature of cryptobioturbation by meiofauna. SB = sequence boundary; TS = transgressive surface; MFS = maximum flooding surface; LST = lowstand systems tract; TST = transgressive systems tract; HST = highstand systems tract.

surfaces within the interval. The biostratigraphy and internal subdivisions were defined by Brett et al. (2004). The descriptions provided for Fig. 2B, C, D, and E are based on outcrop observations, and provide the basis for the more detailed stratigraphic section shown as Fig. 3. Microfacies and facies associations (FA's) in Fig. 3 are based on laboratory examination of polished slabs, thin sections, and SEM imaging.

The base of the section comprises the Lower Portwood (Fig. 2B) which unconformably overlies the Middle Devonian Boyle Dolomite and largely consists of wavy cross-laminated dolarenite beds with variable contents of fossil debris, fish bones, and glauconite. The silty mudstones near the top of the Lower Portwood contain large sand-filled burrows (Fig. 2B) that extend down from the basal dolarenite bed of the Middle Portwood, and have been interpreted as crustacean burrows by Brett et al. (2018). The Middle Portwood is dominated in its lower portion by a sand-silt laminated carbonaceous shale (SLS, Fig. 2C). Millimetre-scale sand-silt layers (Fig. 2C') show lateral thickness variability (pinch-and-swell), may be discontinuous, show scoured bases, and have sharp as well gradational tops. This interval of sand-silt laminated carbonaceous shale is overlain by a thin interval that is characterized by a double ledge of wavy-lenticular dolosiltite beds (DL, Fig. 2A).

Overlying this double ledge, shale sedimentation changes to rhythmic black shales cycles (RBS, Fig. 2D). These cycles have sharp basal contacts that are overlain by black shale that grades upwards into bioturbated mudstone (Fig. 2D'). The Upper Portwood overlies a channelized erosion surface (Fig. 2E), the deepest portions of these channels are filled with a massive weathering dolostone that is overlain by blocky weathering dolostone with softer weathering clay-rich interbeds. A resistant ledge of strongly carbonaceous black shale forms a laterally persistent marker in the middle of the Upper Portwood (Fig. 2E). This ledge is overlain by comparatively thin rhythmic black-gray shales cycles, showing sharp based black shale grading upwards into bioturbated gray mudstone. The number of these cycles changes laterally along the outcrop due to the erosional contact with the overlying Trousdale Member (Fig. 2A).

4. Petrography and sedimentary features of portwood mudstones

Sedimentary components observed in the Portwood mudstone fall into four groups on account of size and origin: 1) silt-to sand-size grains;

2) clayey matrix; 3) diagenetic minerals; and 4) organic matter. Silt to sand-size grains include carbonate particles (dolomite and dolomitized calcite), mud aggregates, quartz, feldspar, mica, metamorphic rock fragments, glauconite and bioclasts (dominantly benthic agglutinated foraminifera, shell fragments and fish scales). In this paper the descriptive philosophy was such that sedimentary components (or grains and particles) form the foundational level of a descriptive hierarchy that leads to microfacies (“building blocks”), which are in turn combined into facies associations (see following section, “facies scheme”)

4.1. Dolomite grains

Dolomite grains in the Portwood Member appear largely to be of detrital origin. Typically, they consist of irregular shaped cores surrounded by overgrowths (Figs. 4 and 5). The core zones of these dolomite grains appear cloudy under the optical microscope (plane light), whereas the overgrowths are clear (Figs. 4A and 5A, C). The size of core zones ranges from several to tens of microns (Fig. 4B and C; Fig. 5). Clays may occur as thin coatings that mark the boundary between cores and overgrowth. Compositionally, cores are mostly dolomite, but may also

be partially calcitic (Fig. 5F). In the majority of cases the overgrowth is dolomite, and thus there is little or no backscatter contrast between detrital core and overgrowth (Fig. 5E). A differentiation is nonetheless possible by way of texture (more inclusions in detrital cores) and charge differences when viewed in secondary mode (e.g. Fig. 4 C).

If dolomite grains occur in a mudstone matrix, overgrowths may be not as conspicuous in transmitted light because many dolomite particles tend to be smaller than the 30 μm thickness of the thin section (Fig. 5E). If viewed under the SEM, however, the overgrowth rims are readily discernible (Fig. 4B and C) and show differential compaction and randomly oriented inclusions of clay flakes, a clear indication that the overgrowth rims formed very early in diagenesis, prior to any compaction, when the original muds were very water-rich. In well-cemented coarser layers, such as thick dolarenite beds (Fig. 4A) and silt layers within mudstones, overgrowths of dolomite grains are rhombic or sub-rhombic, interlocking, and may show single or multiple growth zones (Fig. 4A; Fig. 5A, C). The observations illustrated in Figs. 4 and 5 can be made throughout the Portwood succession, with generally smaller amounts of detrital carbonate observed in the Upper Portwood above the 4.4 m mark (Fig. 3; Table 1). In transport and depositional processes affecting the Portwood Member, detrital dolomite grains play the role typically occupied by quartz and (to a lesser degree) feldspar grains in many other fine grained successions.

4.2. Mud-dominated composite particles

The textural context of a substantial portion of the clays and other fines in the Portwood suggests that they may to a substantial proportion be part of mud-dominated composite particles (MCPs; Li and Schieber, 2018; Li et al., 2020) in the silt to sand grain size range.

4.2.1. Shale lithics

The most easily identified MCPs are shale lithics, composed largely of illite, quartz, feldspar and mica (Fig. 6). Whereas difficult to identify with a petrographic microscope because of similar mineral composition between grain and surrounding matrix, SEM observations allow discrimination of these grains from the matrix. Good indicators are for example a planar internal fabric that is not aligned with the bedding of the shale, and differential compaction of the matrix around these grains, indicating that they were “hard” at the time of deposition. The size of shale lithics in the Portwood ranges from 10 to 30 μm .

4.2.2. Rip-up clasts

Presumed mud rip-up clasts, particles eroded from the contemporary seabed, are substantially more difficult to identify than shale lithics, but nonetheless an important class of MCPs in the Portwood. They consist largely of illite, quartz, dolomite, feldspar, micas, OM and may also contain fine crystalline pyrite (Fig. 7). When contrasted against surrounding rigid grains they appear deformed and squeezed, as well as flattened by compaction. This type of fine-grained aggregates ranges in size from 40 to 100 μm .

4.2.3. Fecal pellets

Another MCP type are pellets of presumed fecal origin. Fecal pellets are produced by organisms that feed in the water column or live in surface sediments. They typically are of oval-flattened appearance due to compaction (Fig. 8A and B), and may also be twisted and squeezed into irregular shapes by surrounding rigid grains during burial and compaction (Fig. 8C and E). Presumed fecal pellets in the Portwood consist of illite, quartz, mica and minor amounts of dolomite and feldspar (Fig. 8A, B and D), and thus are thought to be produced by benthic organisms (Cuomo and Bartholomew, 1991). They are of similar composition as rip-up clasts, but they differ by being better sorted internally and by generally larger size (tens of μm to more than 200 μm) than either shale lithics or rip-up clasts. Some presumed fecal pellets are associated with pyrite framboids and in places with marcasite.

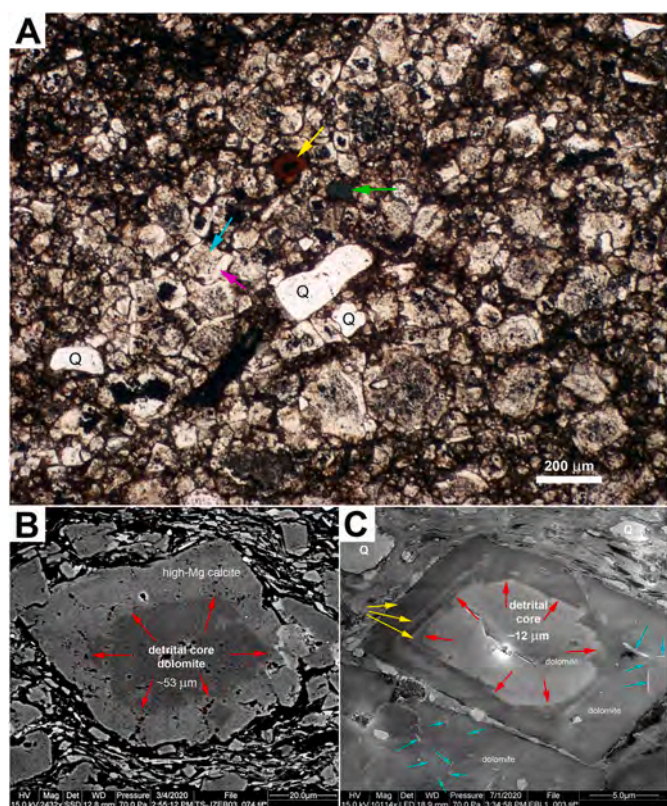


Fig. 4. Detrital carbonate grains in the Portwood Member. (A) Overview of a typical sandy-silty layer. Most of the cloudy appearing grains (cyan arrow) are detrital dolomite or mixtures of calcite and dolomite and have clear overgrowth rims (purple arrow) of variable thickness. Yellow arrow = phosphatic bioclast; green arrow = glauconite, Q = rounded detrital quartz sand. (B) SEM backscatter image of coarse silt detrital dolomite grain (red arrows) in shale matrix with an overgrowth of high-Mg calcite. Differential compaction around dolomite grain indicates early diagenetic formation of overgrowth rim. (C) SEM image (secondary mode) of fine silt size detrital dolomite grain (red arrows) with multiple overgrowth rims (yellow arrows). Note differential compaction of clay matrix. The overgrowth dolomite contains randomly oriented clay flakes (cyan arrows), an indication that this dolomite grew very early in diagenesis when the sediment had a very high water content (ca. 80–90 vol %). (For interpretation of the references to color in this figure legend, the reader is referred to the Web version of this article.)

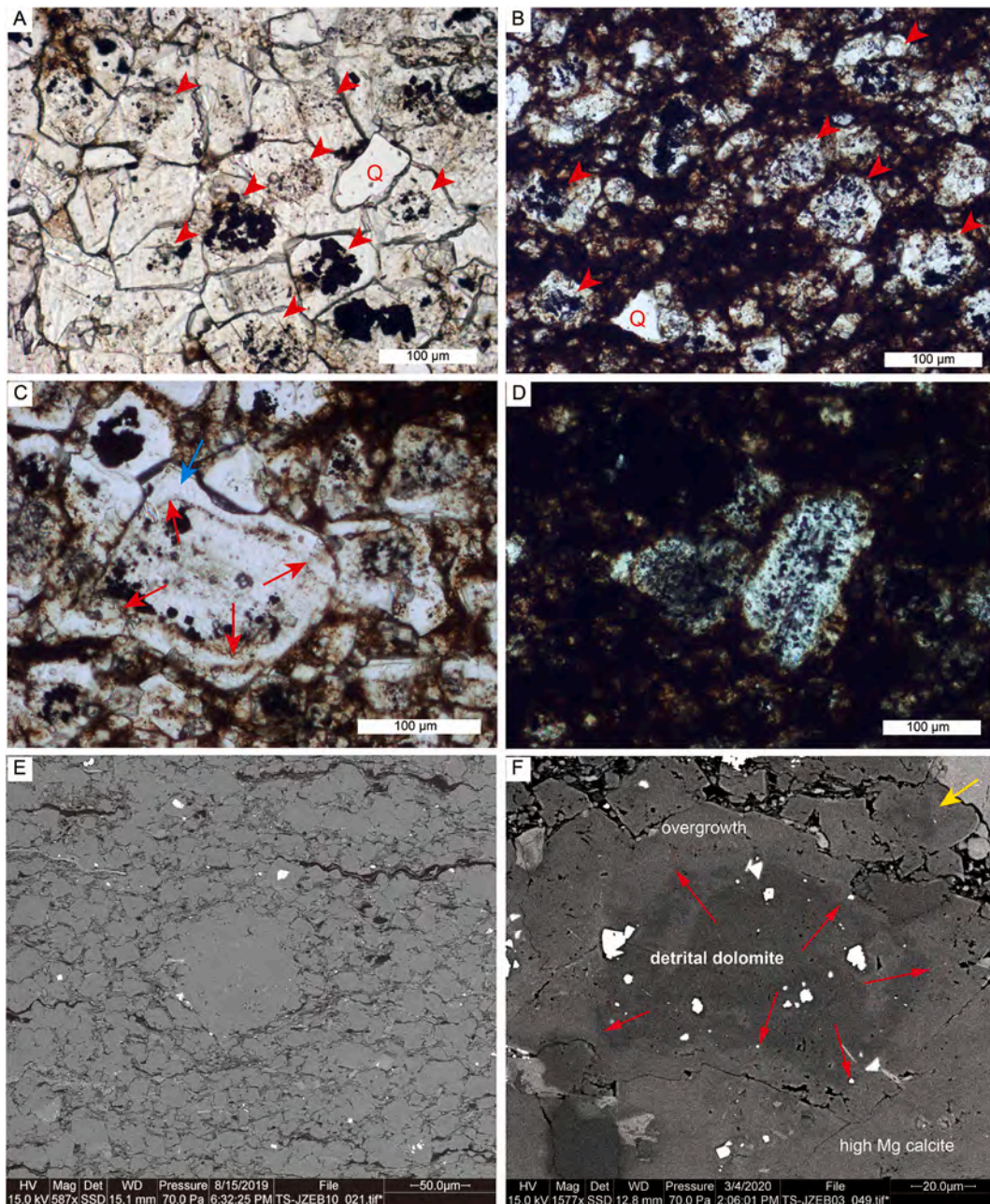


Fig. 5. Detrital carbonate grains in the Portwood Member. (A) Photomicrograph of detrital dolomite (cloudy, red arrows) in a coarse-grained layer with originally open porosity. Shows well developed and interlocking (clear) overgrowth rims. (B) Photomicrograph showing detrital dolomite grains (red arrows) in fine-grained matrix. (C) Closeup of sand-size cloudy detrital dolomite (center, red arrows) with clear overgrowth rim (blue arrow). (D) Sand size detrital dolomite grains in a fine grained shaly matrix. Overgrowth is poorly developed. (E) SEM image (backscatter) of silty mudstone. All the medium gray particles are dolomite, and show detrital cores with overgrowth rims of variable thickness. (F) SEM closeup (backscatter) of detrital dolomite grain (red arrows) that is speckled with high Mg calcite and has a high Mg calcite overgrowth rim. (For interpretation of the references to color in this figure legend, the reader is referred to the Web version of this article.)






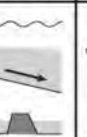


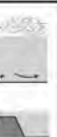








4.2.4. Mud floccules

Above mentioned grain types (siliciclastics, organic matter, bioclasts, rock fragments, glauconite, detrital dolomite and mud-dominated composite particles), however, do not add up to 100%. For given samples, as much as 50% of the rock consists of a mud matrix of uncertain origin, and the question is whether it simply accumulated from a pelagic rain of tiny particles or by some alternative process. Judging from experimental work on mud transport (Schieber et al., 2007; Schieber, 2011a), it seems plausible that mud floccules transported by bottom currents are that missing component. Although rendered “invisible” by compaction under most circumstances (Schieber, 2011a), the fact that larger silt and even sand size particles are intimately mixed with the

“shapeless” mud matrix suggests that not simple settling, but instead co-transport of mud floccules, organic detritus, silt-to sand-size carbonate and siliciclastic grains, and MCPs in bedload via bottom currents is a plausible scenario for transport and deposition (Schieber, 2016a; Yawar and Schieber, 2017; Li and Schieber, 2018). Even though fortunate circumstances are required to recognize mud floccules in the rock record, a subcategory of mud floccules, so-called organo-mineral aggregates (transported marine snow mixed with clay and silt; Kjørboe, 2000; Macquaker et al., 2010), were observed in Portwood thin sections and attest to likely bedload transport of mud floccules (Fig. 9).

Table 1

Summary of sedimentary and compositional elements seen in facies associations (FA's) of the Portwood Member.

Facies Association		Black laminated dolomite-bearing mudstone Dark gray dolomitic mudstone Gray dolomitic mudstone Dolarenite lag Dolarenite Coarse dolosiltite Clayey dolosiltite									
		Abbreviation		SM	LDM	DM	LM	GM	DAL	DA	DS
Element											
Abundance of Sedimentary Features (%)	Silt-sand layers with scoured bases	10-15 (30)								15	
	Silt lenses with scoured bases	0-10 (5)	0-15 (5)		0-15 (5)	0-30 (15)				5	0-10 (5)
	Continuous to discontinuous silt laminae	5-20 (10)	10-25 (20)	15-25 (20)	10-25 (20)	0-20 (10)				15	10-20 (15)
	Compositional banding	40-70 (50)	50-85 (70)	75-85 (80)	50-85 (70)	0-50 (25)				65	70-80 (75)
Carbonate content (%)		16-69 (57)	30-82 (57)	41-64 (54)	11-34 (20)	18-45 (31)	>90	>90	50-82 (72)	51-56 (53)	
TOC (%)		4-15 (7)	1-18 (7)	3-13 (6)	2-16 (6)	0.6-3 (2)	~0	~0	1-3 (2)	0.3	
Bioturbation index (BI)		2-5	1-3	2-4	1-2	4-6	6	6	5-6	4-6	
Ichnofossils		Planolites	Planolites Teichichnus	Planolites	Planolites Chondrites	Planolites	Planolites	Planolites Chondrites	Planolites	Planolites	
Sediment swimmer traces		✓	✓	✓	✓	✓	✓	✓	✓	✓	
Crypto-bioturbation		✓	✓	✓	✓	✓	NR	NR	✓	✓	
Depositional Parameters and Settings											
Explanation of Symbols		wind driven bottom current circulation			storm induced bottom currents			channelized sediment transport			
		storm wave bottom interaction			wave interaction with bottom			relative water depth "deep" to "shallow"			
		bottom waters oxygen limited			seabed buildup shallowing upwards		✓ present	NR not recognized			
numbers in brackets are averages											

4.3. Agglutinated benthic foraminifera

Remains of agglutinated benthic foraminifera (Milliken et al., 2007; Schieber, 2009, 2012) are common in the clay-rich matrix of Portwood samples (Fig. 10). Under the optical microscope and SEM, they appear as collapsed lenticular bodies with a medial suture, ranging in size from 30 to 250 μm . These lenticular bodies are largely composed of tiny detrital quartz grains (1–10 μm in size) that are held together by micro-crystalline quartz cement (Fig. 10C and D). The smaller pieces of this material appear to be fragments of larger lenses. Whereas smaller fragments are a common component throughout the Portwood, intact specimens are most abundant in the uppermost meter of the succession where black and gray shales are rhythmically interbedded (Figs. 2E and 3).

4.4. Organic matter

The Portwood contains abundant amorphous organic matter (AOM) and *Tasmanites* cysts, as well as a minor amount of terrestrial plant debris. Viewed by SEM, AOM is structureless and incorporates clay and silt particles (Fig. 11A and B). *Tasmanites* cysts are flattened by compaction, may be fragmented and broken, and generally are aligned parallel to bedding (Fig. 11C). A small percentage shows various amounts of internal cementation by pyrite, quartz, and carbonate minerals (Fig. 11D). Terrestrial organic matter (TOM, plant debris) is not abundant, but easily identified (Fig. 11A and B) because of internal cellular structural pores (Liu et al., 2017, 2019a, 2019a) and resistance to compaction (deformation of matrix around particles).

5. A facies scheme for the Portwood Member

Shale and mudstone are both widely used terms for fine-grained

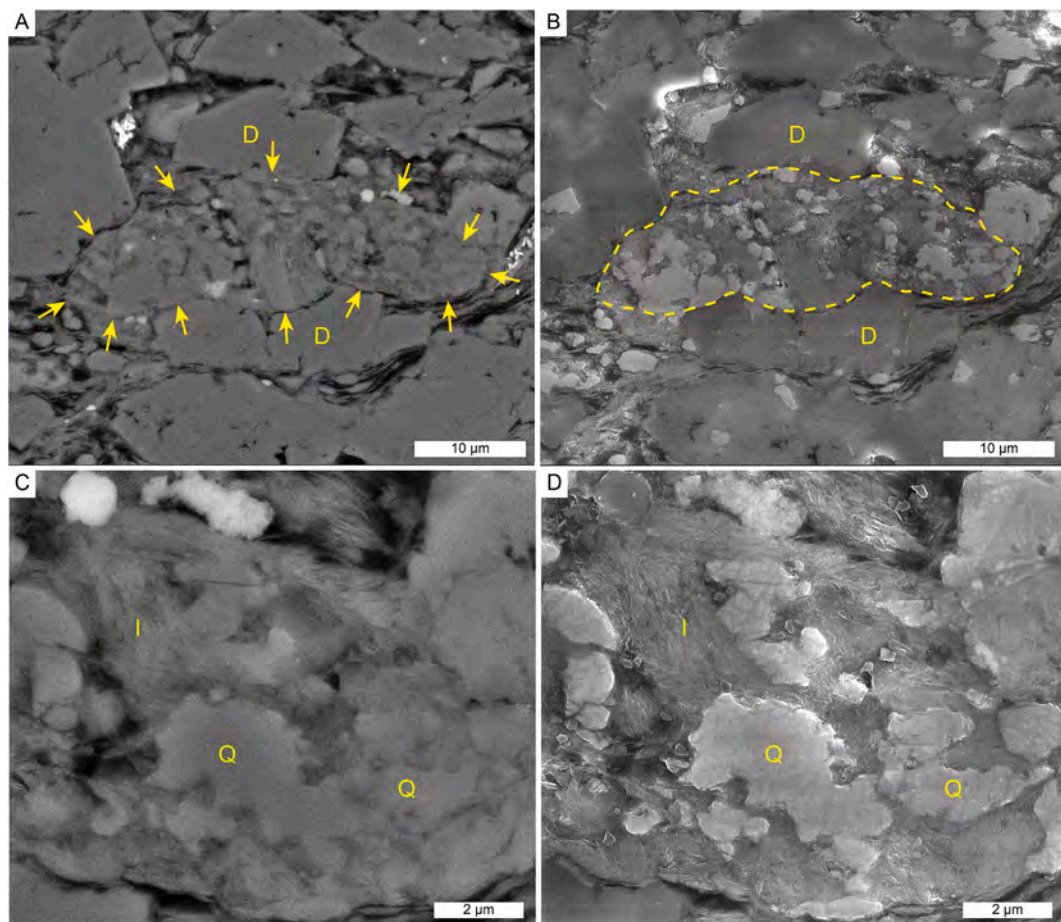


Fig. 6. Lithics are by definition debris from previously formed rocks, and thus hard particles at the time of re-deposition. Figure shows example of shale lithic in the Portwood Shale: (A) Lithic is marked with yellow arrows (SEM backscatter image). (B) Same field of view in secondary electron mode. The lithic is outlined with a yellow dashed line and is composed mainly of illite and quartz. It is compositionally and texturally distinct from the surrounding rock. Had this particle been a soft intrabasinal rip-up clast it would show severe flattening and deformation due to compaction. Images (C) and (D) are textural close-ups from A and B respectively. D - dolomite, Q - quartz, I - illite. (For interpretation of the references to color in this figure legend, the reader is referred to the Web version of this article.)

sedimentary rocks, and whereas there are various approaches to their classification that have been proposed recently (Milliken, 2014; Lazar et al., 2015a, b; Camp et al., 2016), it would be premature to assume that there is a broadly agreed upon terminology for naming and classifying these rocks. Because cm-scale heterogeneity is common to many shale successions, the methodology chosen for this study is to first define the various textural and compositional “building blocks”, such as prominent sedimentary features and layers of distinct composition (e.g. dolosiltite). These “building blocks” can be considered facies or microfacies in analogy with usage for carbonate rocks (Schieber, 1998; Flügel, 2004). At the hand specimen and thin section scale (27 × 46 mm) multiple “building blocks” or microfacies occur closely associated, and on the basis of their relative abundance can then be used to designate facies associations (FA) that facilitate the description of stratigraphic sections (Lazar et al., 2015a, b). “Building blocks” or microfacies elements in the Portwood include (1) sedimentary features, (2) ichnofossils and fabric disruption, (3) layers of distinct composition (e.g. dolosiltite layers), and (4) abundance of carbonate and OM (reported as total organic carbon, TOC), and are summarized in Table 1. Sedimentary features include silt-sand layers with scoured bases, compositional “bands” with gradational-diffused boundaries, continuous and discontinuous silt laminae, and silt lenses with scoured bases (Fig. 12). Silt-sand layers are well cemented layers that consist mainly of coarse (50–500 μm) detrital dolomite grains and quartz, with added feldspar, metamorphic rock fragments, glauconite and bioclasts. They are most common in the lower half of the Middle Portwood mudstone succession. Thickness of single

layers ranges from 1 to 7 mm and thicker layers have a mottled appearance due to fabric disruption by sediment swimmers. Compositional “bands” are a common sedimentary feature throughout the Portwood mudstones and consists of stacked mm to sub-mm thick layers that show gradational transitions to over and underlying layers of differing composition. Because this kind of layering clearly differs from that of well-defined laminae with sharp boundaries we treat it as different, even though this distinction may not be apparent in hand specimen and may need thin section examination for identification. Silt laminae and lenses are typically one to several grains thick, and thinner and finer grained than silt-sand layers. All of the above sedimentary characteristics were observed throughout the Portwood succession.

Ichnofossils in the Portwood were first described by Jordan (1985), who mentioned *Planolites*, *Chondrites*, *Zoophycus*, *Teichichnus*, *Trichichnus*, *Rhizocorallium*, *Phycodes*, and *Laevicyclus*. By far the most commonly observed trace fossils are *Planolites* and sediment swimmer traces. The former are filled with detrital grains from overlying beds, whereas the latter were produced when organisms moved through surficial muds with water contents of 70 vol % or more (“mantle and swirl” structures, Lobza and Schieber, 1999). In addition to disruption of primary layering by *Planolites* and sediment swimmer traces, cryptobioturbation, fabric disturbance by sub-mm size benthic organisms (tiny worms, benthic foraminifera; Pike et al., 2001; Bernhard et al., 2003; Löhr and Kennedy, 2015), is a major contributor to the disruption and erasure of laminae and layer boundaries (Fig. 13).

The relative abundances of microfacies elements in the Portwood are

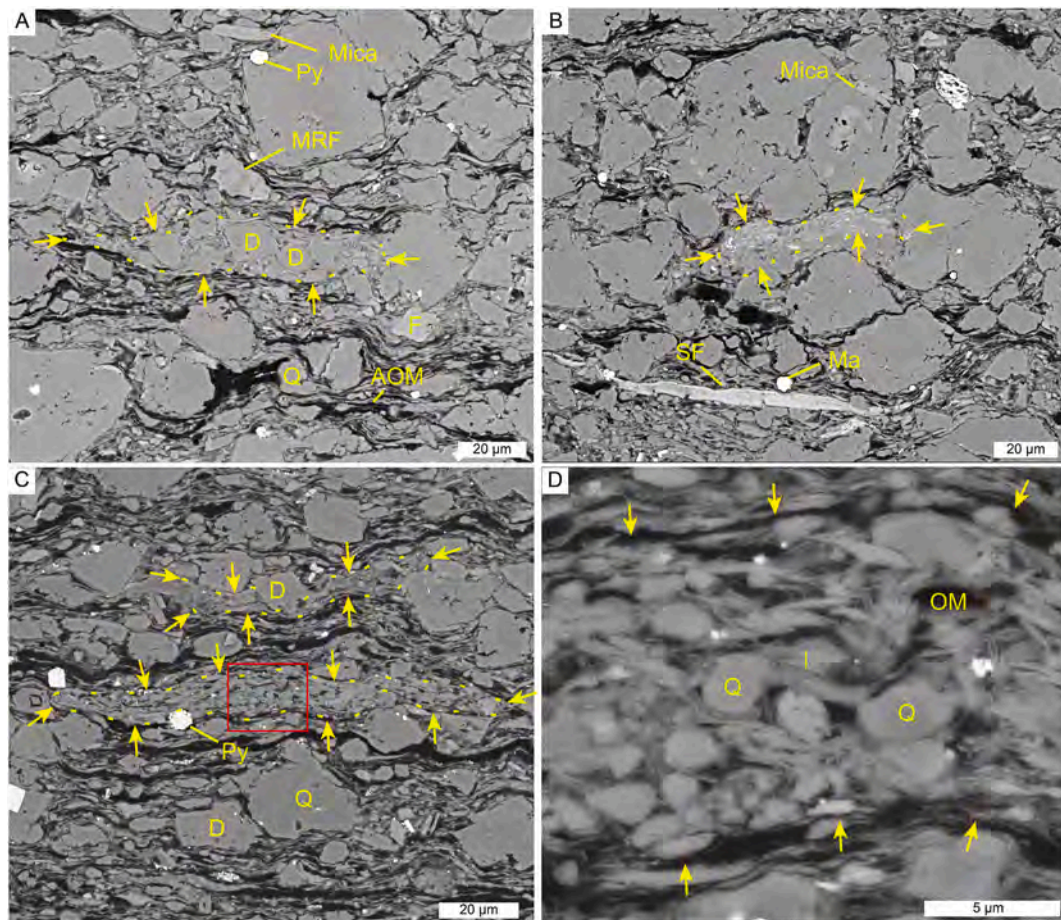


Fig. 7. Presumed rip-up clasts in the Portwood Shale: A) SEM image (backscatter) showing deformed and compacted rip-up clast (outlined with wide-space dashed yellow line and yellow arrows) composed of euhedral dolomite grains (marked D), quartz and illite; B) SEM image (backscatter) showing deformed and compacted rip-up clast (outlined with wide-space dashed yellow line and yellow arrows) consisting of illite, quartz, phosphate and marcasite. C) SEM image (backscatter mode) showing deformed and compacted rip-up clasts (outlined with wide-space dashed yellow line and yellow arrows) composed of illite, quartz, mica and organic matter; D) enlarged view of red rectangle in C that shows compacted clay (illite) fabric. Yellow arrows mark textural boundary between compacted rip-up clast and surrounding material. D = dolomite, F = feldspar, MRF = metamorphic rock fragment, OM = organic matter, AOM = amorphous organic matter, Py = pyrite framboid, Q = quartz, SF = shell fragment (phosphatic), Ma = marcasite. (For interpretation of the references to color in this figure legend, the reader is referred to the Web version of this article.)

summarized in Table 1. Groupings of these that are recurring and comparatively abundant have been designated as facies associations (FA) in Table 1.

A total of nine FA's have been recognized in the Portwood (Table 1): (1) sandy-silty black dolomitic mudstone (SM); (2) black laminated dolomitic mudstone (LDM); (3) dark gray dolomitic mudstone (DM); (4) black laminated dolomite-bearing mudstone (LM); (5) gray dolomitic mudstone (GM); (6) dolarenite lag (DAL), (7) dolarenite (DA) (8) coarse dolosiltite (DS); and (9) clayey dolosiltite (CDS). Their characteristics are described below.

The sandy-silty black dolomitic mudstone (SM) FA dominates the bottom portion of the Portwood succession (Fig. 3), and is characterized by sandy-silty layers with scoured bases that are interbedded with dark clay-rich layers (Figs. 12 and 14). The well cemented sandy-silty layers consist mainly of detrital carbonate/dolomite grains, with addition of detrital quartz, feldspar, metamorphic rock fragments and bioclasts. Sandy-silty layers are 1–7 mm thick, and show mottled texture as well as relict normal grading. In addition, abundant well-rounded quartz sand grains occur in these layers and in burrow fills (Fig. 15 A and B). Some of the well-rounded quartz sand grains show one or two generations of quartz overgrowth. In grains with two generations of overgrowths, the first-generation overgrowth is typically abraded-rounded and the second generation shows irregular-euhedral outlines (Fig. 15C and D).

Bioturbation intensity in the SM FA varies from moderate to strong (BI = 2–5), with fabric disruption caused by sediment swimmer traces (“mantle and swirl” structure, Lobza and Schieber, 1999), and *Planolites* burrows filled with detrital grains. The clay-rich interbeds of the SM FA show cryptobioturbation expressed as sub-mm scale disruption of laminae and compositional “bands” with gradational boundaries between adjacent layers.

Whereas the SM FA dominates the basal meters of the Portwood succession, at approximately 1 m above the base the black laminated dolomitic mudstone (LDM) FA, the overall most abundant FA in the Portwood (Fig. 3), becomes increasingly common (Fig. 16). The LDM FA is highly variable in carbonate and OM content (Table 1). Sedimentary structures in this facies are dominated by compositional “bands” and thin silt laminae and silt lenses (Fig. 16B and C). The uppermost meter of the Middle Portwood consists of rhythmic LDM and DM couplets (Figs. 2D and 3), with sharp-based beds of LDM FA passing upwards into DM FA. The DM FA shows similar sedimentary structures as the LDM FA, but is less black, more bioturbated, and weathers somewhat recessive (Fig. 2D). The DM FA has a slightly higher carbonate content and lower TOC content compared to the LDM FA that it is interbedded with (Fig. 3). Both FA's show bioturbation, but the BI of the DM FA is higher than that of the LDM FA (Fig. 16). Prevalent crypto-bioturbation in these FA's is expressed as mottling of silt laminae and clay-rich matrix

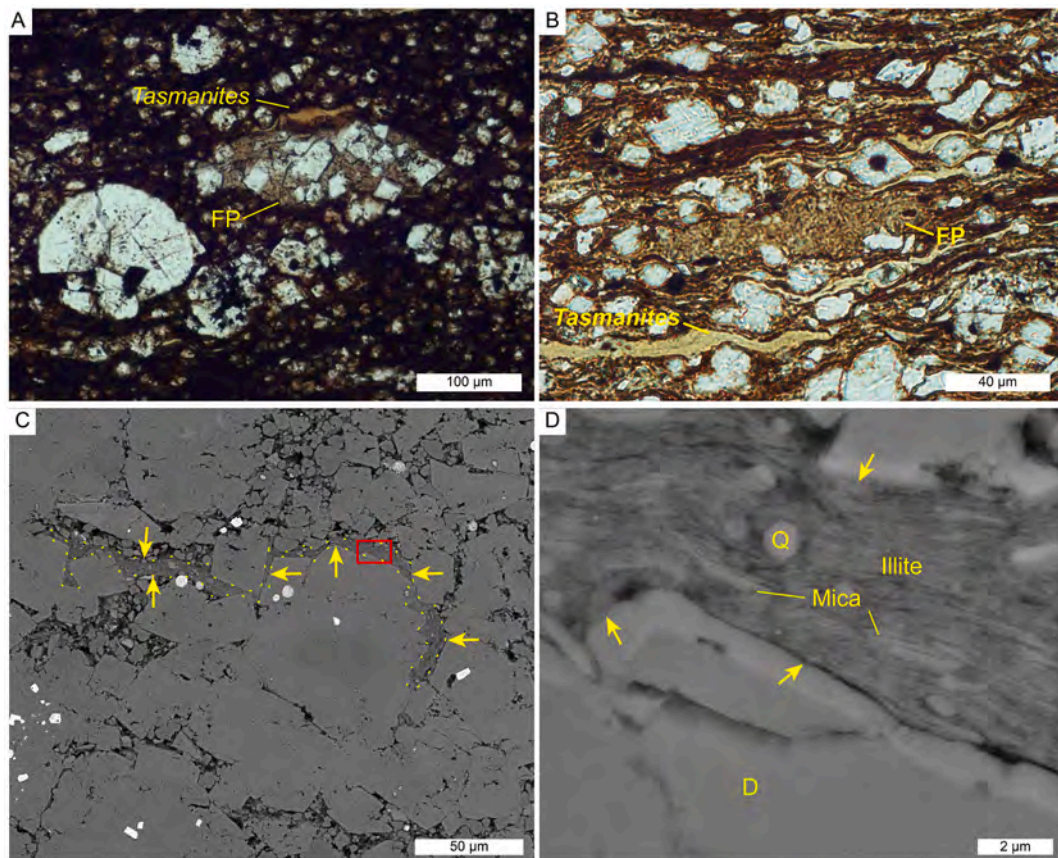


Fig. 8. Presumed fecal pellets in the Portwood Shale: A), B) Photomicrographs (plane light) showing variably deformed compacted pellets (FP). C) elongated pellet (outlined with wide-space dashed yellow line and yellow arrows) strongly deformed between surrounding rigid grains; D) close up of red rectangle in C with strongly compacted clay fabric. Yellow arrows point to textural boundary between pellet and surrounding mineral grains. D = dolomite, Q = quartz. (For interpretation of the references to color in this figure legend, the reader is referred to the Web version of this article.)

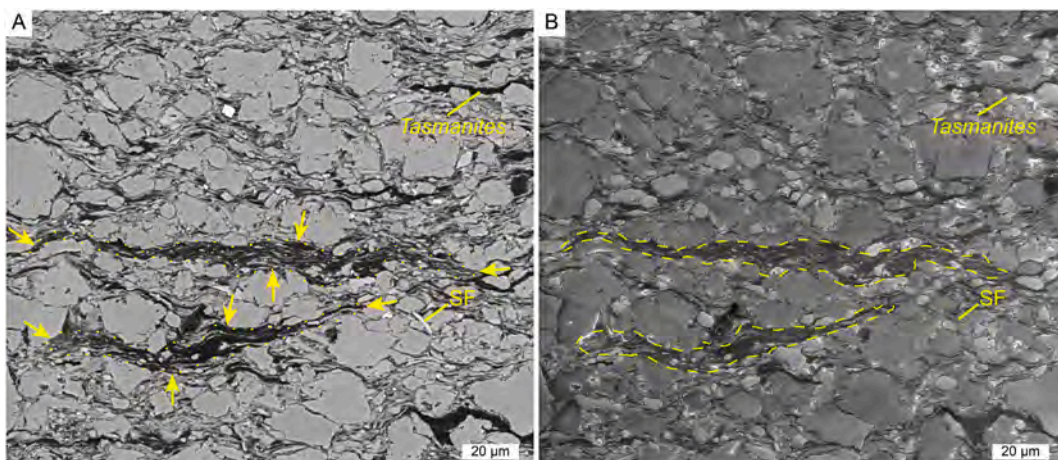


Fig. 9. SEM images (A = backscatter electron mode; B = secondary electron mode) that show organo-mineral aggregates (dashed yellow lines) with abundant organic matter. Although not abundant in Portwood thin sections, they do suggest transport of flocculated particles together with other aggregate grains. SF-shell fragment. (For interpretation of the references to color in this figure legend, the reader is referred to the Web version of this article.)

(Fig. 16A and B).

The LM FA is prominent in the upper half of the Upper Portwood (Figs. 2 and 3). Although of very similar appearance in hand specimens, when compared to the LDM FA it has a distinctly lower carbonate content (Table 1). The size of detrital dolomite grains in the LM FA is generally smaller than observed in other FA's. Readily observable sedimentary structures are mainly thin silt laminae and silt lenses with

scoured bases, and macroscopic sedimentary features are overall less conspicuous than in the LDM FA. In addition, bioturbation features (Fig. 17B and C) are more subtly expressed (BI = 1–2) than in other FA's in the Portwood succession.

The GM FA consists of layers of gray to greenish gray dolomitic mudstones that form depositional couplets with interbedded layers of the LM FA in the Upper Portwood succession (Figs. 2E and 3).

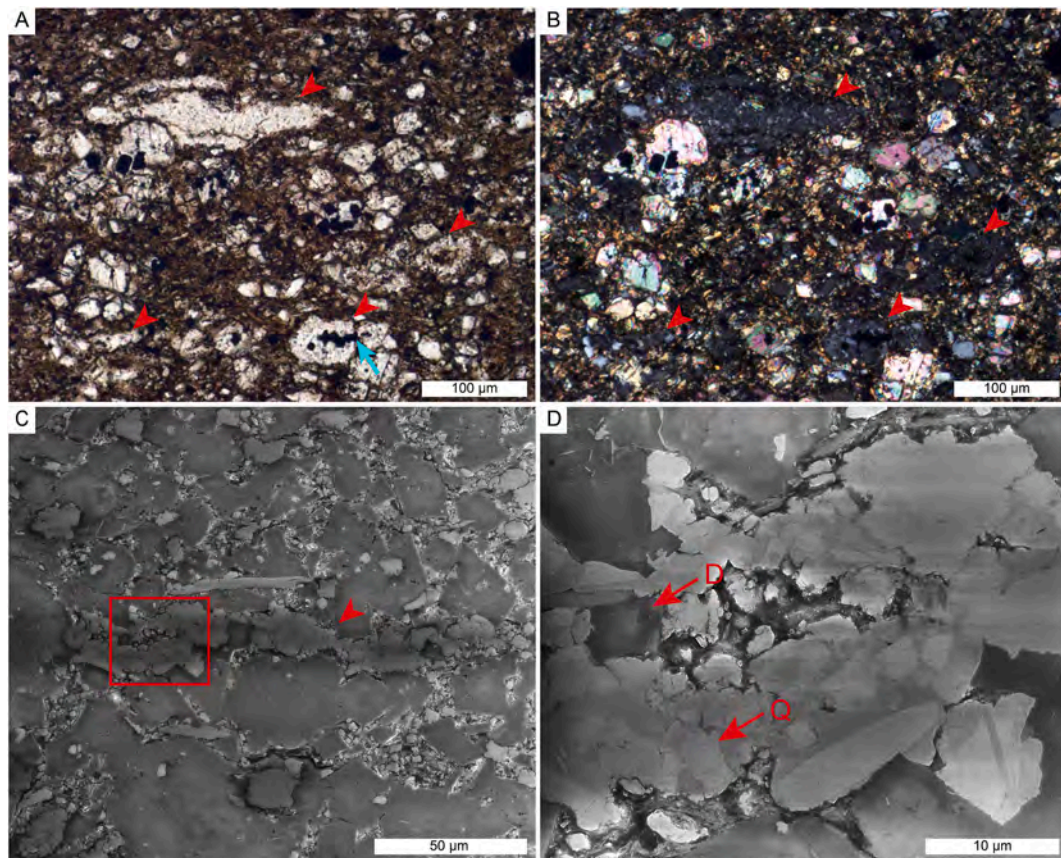


Fig. 10. Agglutinated benthic foraminifera: (A) and (B) Photomicrograph (A = plane- and B = cross-polarized light) that shows agglutinated benthic foraminifera (red arrows) composed of tiny detrital quartz grains and microcrystalline quartz cement; (C) SEM image (secondary electron mode) of agglutinated benthic foraminifera (red arrows); (D) Closeup of red rectangle in C, showing foraminiferal test composed of small quartz grains (light gray, red arrow) that are cemented by diagenetic silica (darker gray, yellow arrow). (For interpretation of the references to color in this figure legend, the reader is referred to the Web version of this article.)

Rhythmically deposited couplets (Fig. 2E) consist of sharp-based beds of the LM FA passing upwards into the GM FA. The GM FA has a higher carbonate content and a lower TOC content relative to the interbedded LM FA (Table 1). As observed in other Portwood FA's, the majority of dolomite grains shows cloudy "cores" and irregular outlines, and a subset of dolomite grains has euhedral rhombic outlines and lacks internal "cores". AOM is very low in the clayey matrix of the GM facies, which in places also shows thin marcasitic lags. The GM FA generally appears homogeneous and massive, and only remnants of primary bedding can be observed in polished slabs (Fig. 17A and C). In GM FA samples that have relatively low carbonate content, sedimentary features such as silt laminae and silt lenses are more common. Any primary sedimentary fabrics of the GM FA have been extensively disrupted by burrowing benthic organisms (BI = 4–6). Burrows, sediment swimmer traces and cryptobioturbation are pervasive (Fig. 17).

Light gray to gray dolomitic layers that are associated with above mudstone FA's are FA's DAL (dolarenite lag), DA (dolarenite), DS (coarse dolosiltite) and CDS (clayey dolosiltite), illustrated in Figs. 18 and 19. The thickness of these dolomite rich FA's ranges from 1 to 85 cm. DAL and DA FA's are fully bioturbated (BI = 6) and of massive appearance (Fig. 19A and B). They consist mainly of detrital dolomite grains (20–300 μm) and minor detrital quartz (10–400 μm), and are held together by diagenetic carbonate cement. TOC levels are below detection limit. A significant amount of sand-size grains in the DA FA have recrystallized to dolomite (Fig. 19E). Shell fragments and ooids are abundant in the DAL FA (Fig. 19F and G). Due to extensive bioturbation, primary sedimentary features are rarely preserved. Numerous sediment swimmer traces and successor burrows (*Chondrites*, *Planolites*, etc.)

dominate the appearance of these FA's in polished slabs. DS and CDS FA's display strongly mottled to homogenous textures (Figs. 18 and 19C and D). Framework grains consist of detrital dolomite, quartz, glauconite, and bioclasts. Both DS and CDS FA's are low in TOC content (Table 1) and primary sedimentary structures have been heavily disrupted by sediment swimmers (BI = 4–6), but CDS shows more preserved primary sedimentary fabrics (Fig. 19D). Outcrop studies of the Portwood by other researchers reported large *Cruziana* type burrows at the base of the Middle Portwood, as well as *Zoophycus* and *Trichichnus* in Upper Portwood clay-rich dolostones (Brett et al., 2018).

6. Discussion and interpretation of observations

6.1. Provenance of detrital carbonate and siliciclastic grains

Thrust-loading of the Acadian Orogeny led to the uplift of the Cincinnati Arch to the west of the Appalachian basin, producing several large unconformities on the cratonward side of the basin (Ettensohn, 1994; Smith et al., 2019). Towards the west, sediments become thinner, more organic-rich, and pinch out on these unconformities (Smith et al., 2019). The unconformity that separates the Portwood Member from the underlying Boyle Dolomite is equivalent to the second-order Taghanic unconformity, which is associated with erosion of underlying carbonate strata on a regional scale (Brett et al., 2018). The Portwood Member appears to have received clastic inputs from multiple sources. Detrital quartz silt, feldspar, mica, metamorphic rock fragments and shale lithics were most plausibly derived from the Acadian Orogen to the east (Ettensohn, 1985; Ettensohn et al., 1988). Concerning the origin of

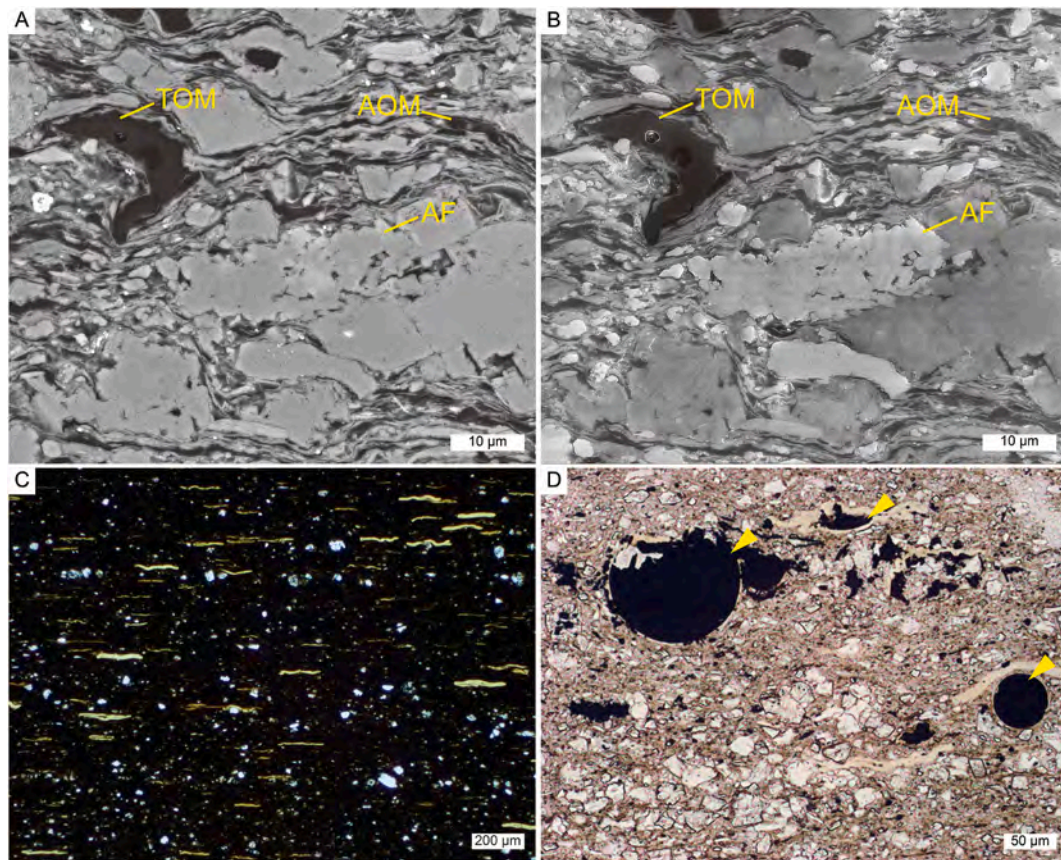


Fig. 11. Organic matter in the Portwood Shale: (A) Secondary electron SEM image of mudstone fabric with streaks of amorphous organic matter (AOM) interwoven with clays and silt, and a particle of terrestrial organic matter in the center (TOM). The latter shows structural pores and resists compaction (differential compaction around particle). (B) Another example of a compaction resistant particle of TOM. (C) Photomicrograph (plane-polarized light) that shows abundant compacted *Tasmanites* cysts (yellowish-brown) aligned parallel to bedding; (D) Photomicrograph (plane-polarized light) that shows uncompacted *Tasmanites* cysts (red arrows) filled with early diagenetic pyrite (Schieber and Baird, 2001). (For interpretation of the references to color in this figure legend, the reader is referred to the Web version of this article.)

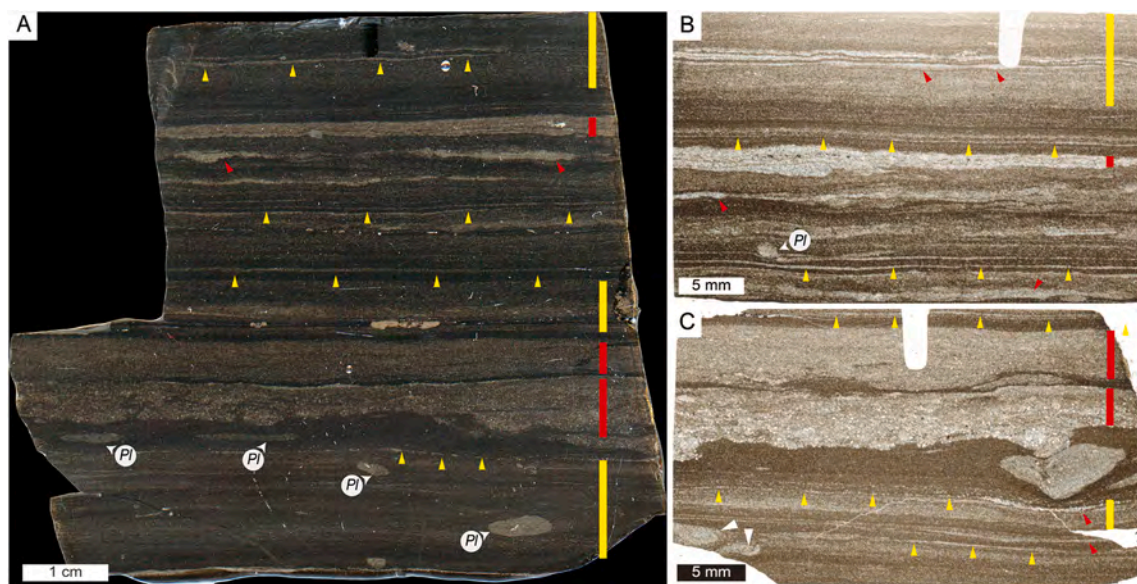


Fig. 12. Sedimentary features of the Portwood mudstones (FA SM): (A) Image of polished slab showing abundant silt-sand layers with scoured bases (red bars), silt lenses with scoured bases (red arrows), continuous to discontinuous silt laminae (yellow arrows), and compositional banding (yellow bars). (B) Thin section cut from the upper part of the slab at left, showing abundant sedimentary features and common bioturbation. (C) Thin section cut from the lower part of the slab on the left, showing details of sedimentary features and bioturbation. *Planolites* (white arrows, PL) and sediment swimmer traces (white arrows) are most common. Burrows are typically filled with silt/sand-size grains. (For interpretation of the references to color in this figure legend, the reader is referred to the Web version of this article.)

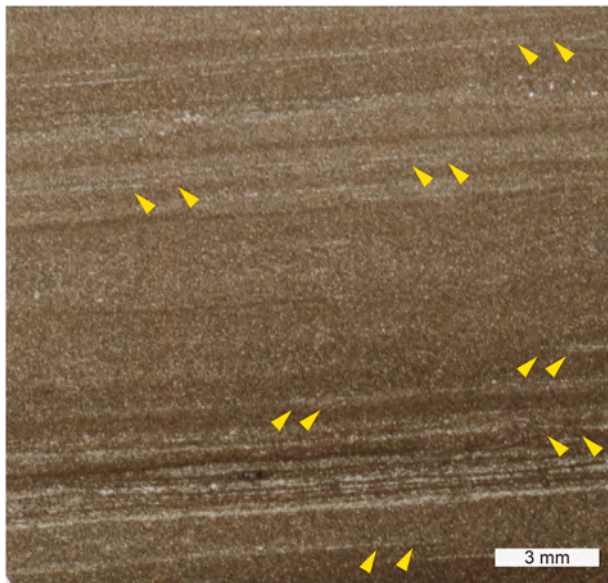


Fig. 13. Thin section scan image showing extensive cryptic bioturbation. Homogenized fabric and blended silt laminae (arrows), probably caused by minute benthic organisms.

recycled carbonates, such components have been described from a variety of other sedimentary successions (Amsbury, 1962; Lindholm, 1969; Milliken and Land, 1993; Taylor et al., 2000; Martire et al., 2014), but in most instances their abundance is on the order of a few percent because their survival into the marine realm is limited by their comparative softness and solubility in the course of outcrop weathering and transport. The strong dominance of recycled carbonate grains in the detrital fraction of the Portwood Member (Fig. 4) therefore suggests derivation from a carbonate dominated source area and a comparatively short transport path. Uplifted blocks of underlying carbonates (Boyle Formation and older) that formed scattered islands in what is now central Kentucky are therefore the most likely sources for detrital carbonate (largely dolomite) grains (Schieber and Lazar, 2004; Brett et al., 2018). Whereas the original input of detrital carbonates may have been a mixture with abundant calcitic particles, partial dissolution of carbonate particles during early diagenesis would have preferentially affected calcitic particles because of the lower solubility of dolomite (Garrels,

1960; Langmuir, 1997), and may have caused the now observed strong dominance of detrital dolomite grains. Early diagenetic framboidal pyrite is ubiquitous in the Portwood (Fig. 7), and testifies to bacterial sulfate reduction in sediments near the sediment water interface. In combination, dissolution of calcitic grains, sulfate reduction, and concomitant increase in alkalinity should have led to precipitation of early diagenetic dolomite cements (Baker and Kastner, 1981; Compton, 1988; Kastner et al., 1990), an expectation that is borne out by petrographic observations of Portwood samples (Figs. 4 and 5). Thus, not only the still identifiable detrital carbonate particles, but also a substantial portion of the carbonate (dolomite) cement in the Portwood may ultimately be (via chemical recycling) of detrital origin.

Whereas silt-size quartz grains in the Portwood probably reflect input from an eastern source (Schieber, 2016), the well-rounded quartz sand grains (Fig. 15) in sandy layers and burrow infills in the lower part of the outcrop (FA SM) are in sharp contrast to the other siliciclastic components with regard to rounding and sphericity. The general implication of that type of quartz grains is one of long residence time on a cratonic surface, tectonic quiescence (Folk, 1980), an episode of aeolian reworking (Kuenen, 1960; Dott, 2003) or multiple cycles of transport (Pettijohn et al., 1987), conditions that make an association with the Acadian Orogen unlikely. By petrographic comparison with pre-Devonian sandstone units of the mid-continent region of the USA, the observed sand grains compare well with those typical for the Ordovician St. Peter Sandstone (Mazullo and Ehrlich, 1983; Dott, 2003), an extensive cratonic sand sheet that extends at least as far east as central Indiana (Gray et al., 1987). Given that Middle and Upper Devonian black shale units onlap unconformities on tectonic highs to the west (Smith et al., 2019), it seems sensible to associate the well-rounded quartz grains in the lower Portwood with erosion of older strata to the west, preceding the eustatic sea level rise known as the Taghanic Onlap (Johnson et al., 1970), which resulted in deposition of the Portwood Member in Kentucky (Brett et al., 2018). The observation of abraded overgrowth rims on these quartz grains (Fig. 15) is decisive evidence for recycled quartz grains (Pettijohn et al., 1987) and suggests a link to a distal unconformity (Basu et al., 2013), consistent with above interpretation.

6.2. Processes of sediment transport and environments of deposition

In their stratigraphic analysis of the Portwood Member, Brett and his co-workers (Brett et al., 2004, 2018) suggests a variably shallow depositional setting. In this study, observations made in polished slabs and

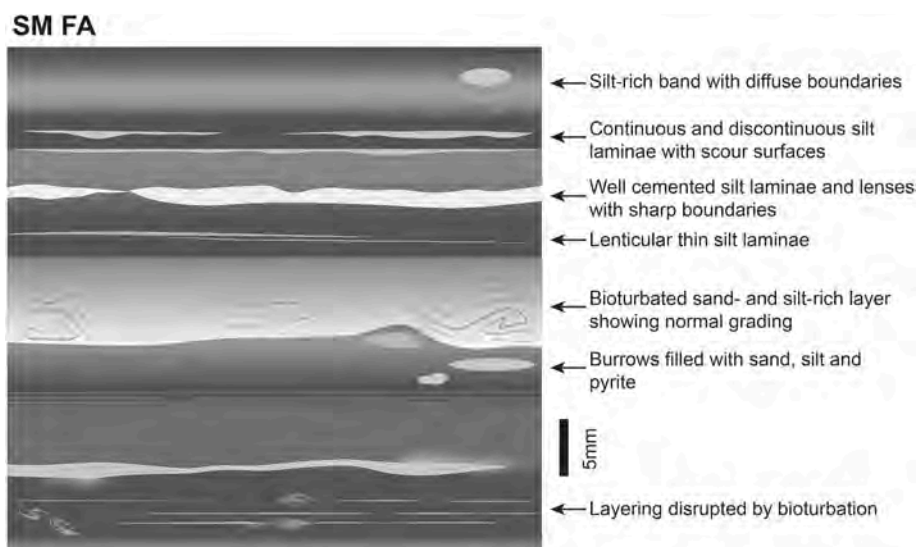


Fig. 14. Line drawing that summarizes features observed in the SM FA.

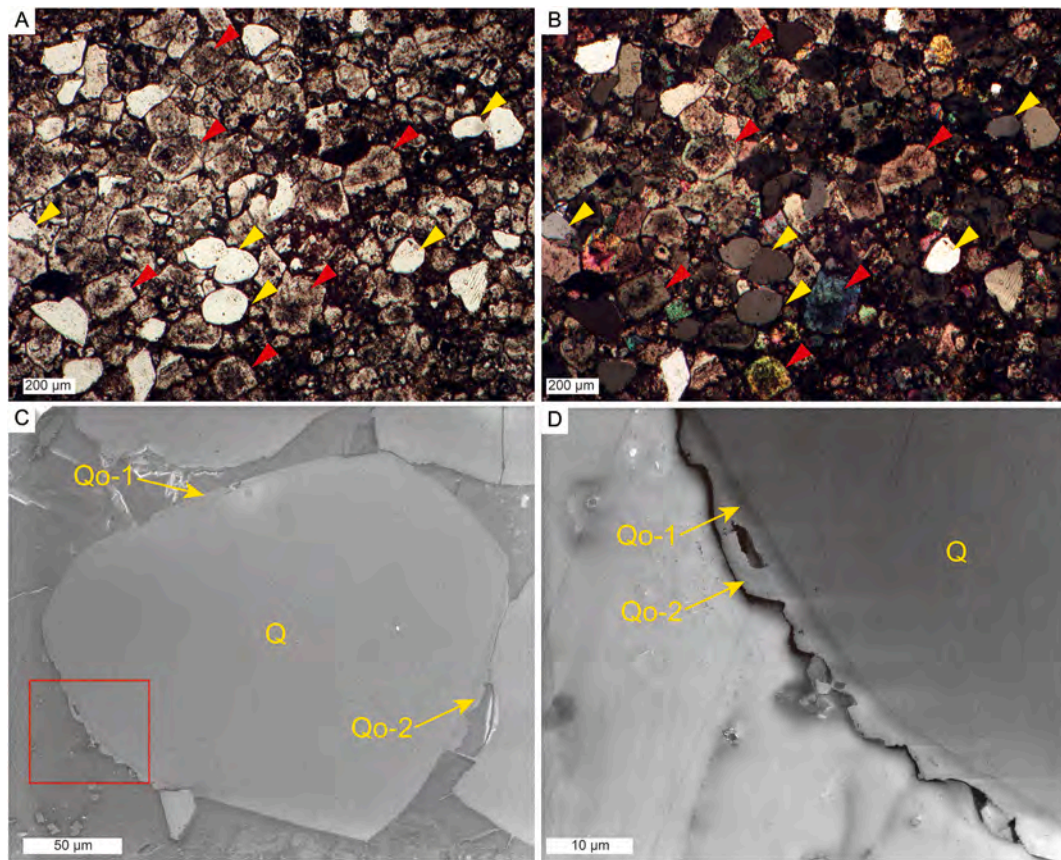


Fig. 15. A), B) Photomicrographs (plane and cross-polarized light) showing detrital dolomite (red arrows) and well-rounded quartz (yellow arrows) in sandy-silty layers of the SM FA; C) SEM image (secondary electron mode) of well-rounded quartz with overgrowths; D) closer view of red square in C, showing two generations of overgrowth. Q-original quartz grain, Qo-1-first generation overgrowth, Qo-2-second generation overgrowth. (For interpretation of the references to color in this figure legend, the reader is referred to the Web version of this article.)

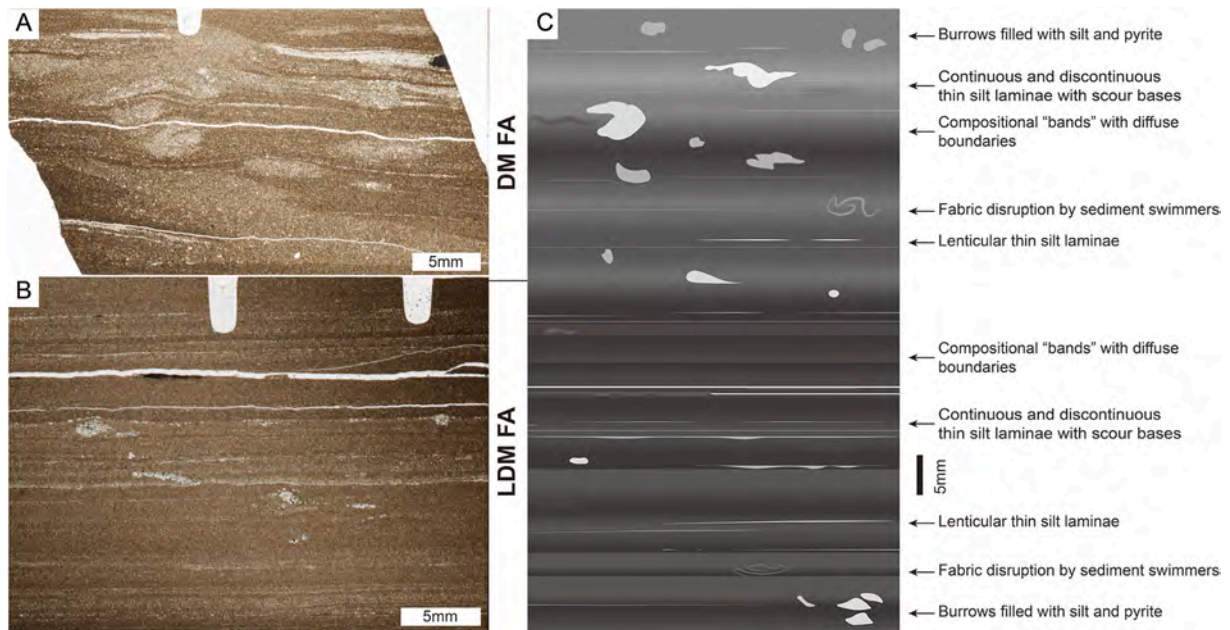


Fig. 16. Thin section scans (A and B) and line drawing (C) that summarize features observed in the black laminated dolomitic mudstone (LDM) and dark gray dolomitic mudstone (DM) FA's.

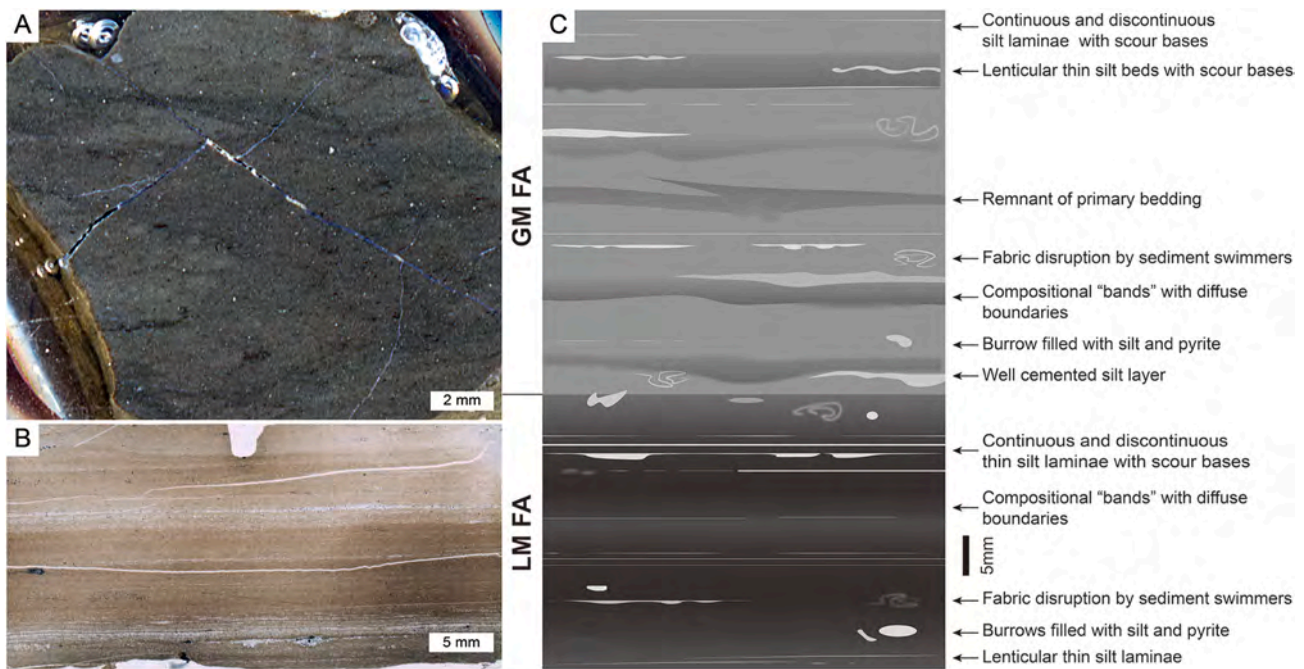


Fig. 17. Rock slab (A), thin section scan (B), and line drawing (C) that summarize features observed in the LM and GM FA's.

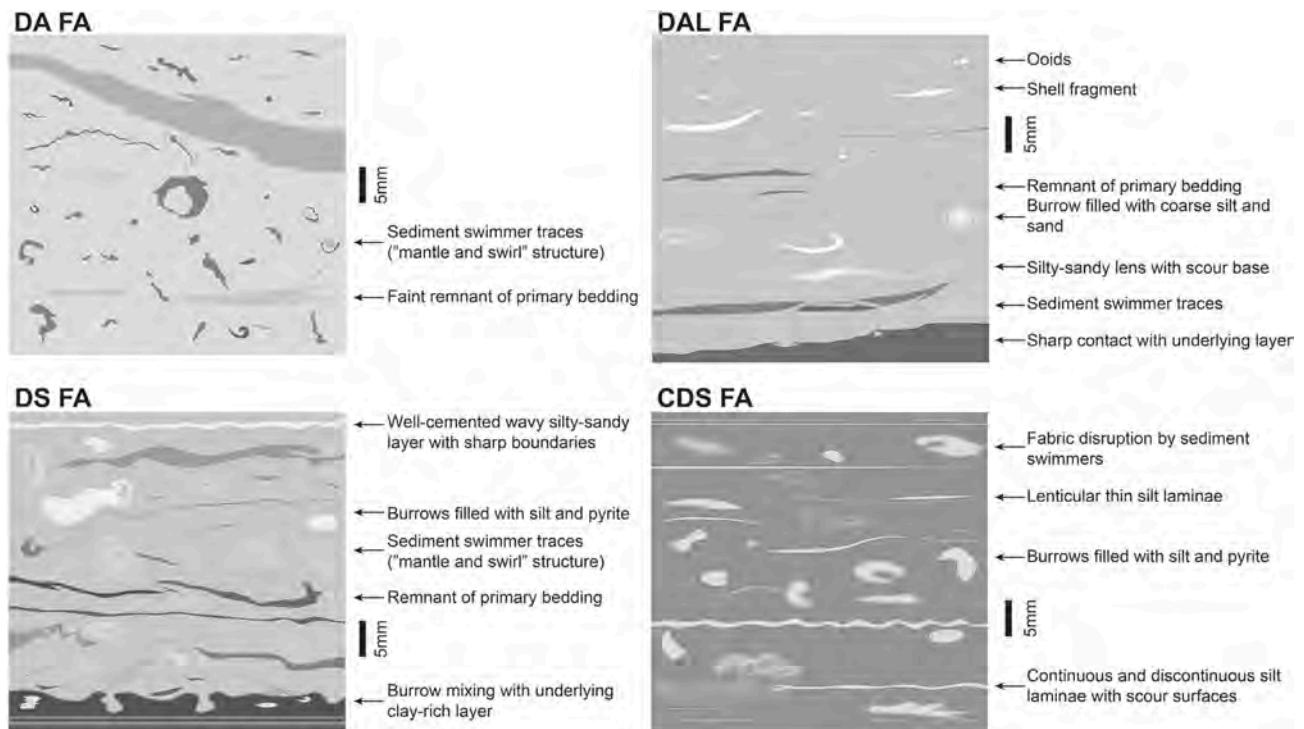


Fig. 18. Line drawings that summarize features observed in the dolarenite (DA), dolarenite lag (DAL), coarse dolosiltite (DS) and clayey dolosiltite (CDS) FA's.

thin section additionally suggest a likely prevalence of sediment transport and dispersal by bottom currents.

In FA SM, sandy-silty layers with detrital dolomite, erosive bases, normal grading, and various degrees of bioturbation (Figs. 12 and 14) resemble storm deposits observed in other fine grained successions (Schieber, 1990, 1999, 2003, 2003; Ghadeer and Macquaker, 2011; Trabucho-Alexandre, 2014). Given their thickness (up to 7 mm) and composition (detrital dolomite), as well as being located on the eastern flank of the Cincinnati Arch (Fig. 1), these layers were likely derived

from a nearby source, such as exposed portions of the Cincinnati Arch, and uplifted, island-forming, blocks of older carbonate strata, rather than from the margin of the Appalachian Basin, several 100 km's to the east. The presence in these layers of rounded quartz grains that were likely derived from older strata that were contemporaneously eroded further west (Smith et al., 2019), suggests mixing of terrestrial inputs and local carbonate debris, possibly by storm-induced basinward flowing bottom currents (Aigner and Reineck, 1982; Allen, 1985; Schieber, 2016b).

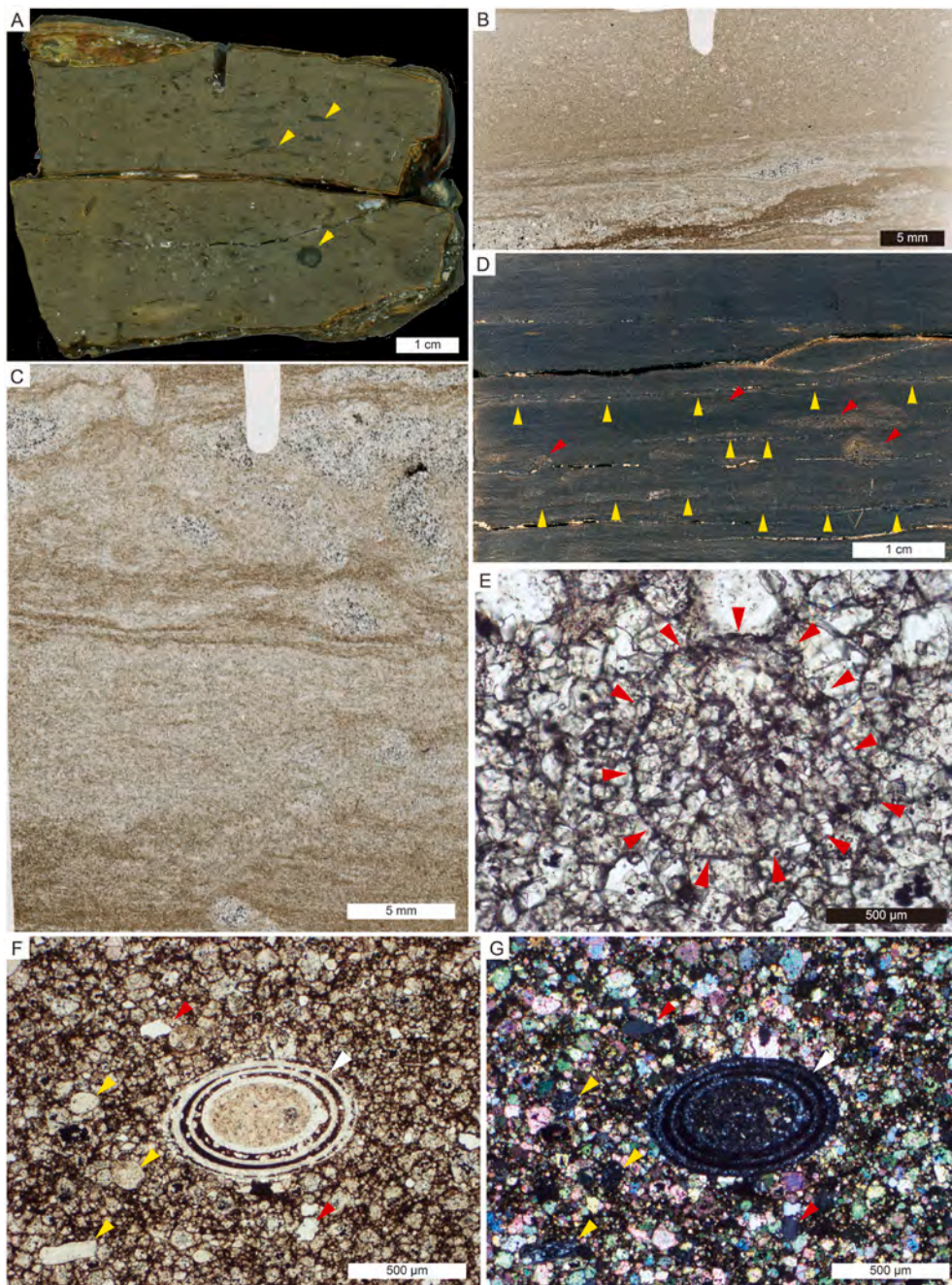


Fig. 19. A) Polished slab of the DA FA, showing abundant burrows and sediment swimmer traces (yellow arrows). B) Thin section scan from the DAL FA, showing mottled to homogenized fabric. C) Thin section scan from the DS FA. The fabric is disrupted by sediment swimmers, and the basal contact with the underlying clay-rich mudstone is bioturbated. D) Thin section scan from the CDS FA, showing sharp-based silt laminae (yellow arrows), silt filled burrows (red arrows) and mottled texture. E) Photomicrograph of the DA FA (plane-polarized light), showing a recrystallized sand-size detrital dolomite grain (red arrows). F) and G) Photomicrographs (plane and cross-polarized light) showing the DAL FA composed of detrital dolomite, scattered detrital quartz (Q, red arrows), ooids (silicified, white arrow) and shell fragments (yellow arrows). (For interpretation of the references to color in this figure legend, the reader is referred to the Web version of this article.)

Well cemented silt laminae and lenses with sharp boundaries (Figs. 12 and 14), as well as the thin parallel to lenticular silt laminae with interbedded muddy laminae (Yawar and Schieber, 2017), can be interpreted as generic bottom current deposits (Schieber, 2016b). Contrasting intervals with 1) abundant evidence of current transport and 2) slower deposited meiofaunally reworked laminae (compositional “bands”; Schieber and Lazar, 2004; Spencer, 2013; Riese, 2014) suggests a dynamic shallow water setting.

In FA LDM, silt laminated black shale (Fig. 16) indicates common bottom current activity and bedload transport of silt and mud floccules (Schieber et al., 2007; Yawar and Schieber, 2017). Interspersed compositional “bands” and cryptobioturbation suggest slower deposited muds that may have been laminated prior to meiofaunal reworking. Compared with FA SM, the LDM FA suggests somewhat lower energy conditions and possibly deeper water than the SM FA.

Cyclic succession from FA LDM to DM shows the same primary

sedimentary features (lamination) in both FA's, but there is distinctly more macroscopic bioturbation in the DM FA. The gradational transition from LDM to DM (Figs. 2 and 3), the sharp base of LDM beds, and the upwards decrease of TOC content in these cycles (Fig. 3) suggest that these cycles may represent shallowing upwards parasequences. Prior to compaction (assuming 80–90 vol% water content) these cycles (Fig. 3) would have been from 1 to 4 m in thickness. A model presented by Spencer (2013) posits that in generally shallow water settings, a sediment buildup of that magnitude would have progressed from deeper and poorly aerated conditions to shallower conditions with better oxygen supply from surface waters towards the top of the cycle.

Comparable depositional cycles, consisting of sharp-based LM beds that grade upwards into bioturbated GM (Fig. 18), occur in the upper half of the Upper Portwood, (Figs. 2 and 3). In comparison to LDM-DM cycles, the upper part of LM-GM cycles is distinctly more bioturbated (Fig. 18) and lower in TOC content (Fig. 3), suggesting better

oxygenation and probably shallower water depth for the upper half of these cycles.

The various dolomitic FA's (Fig. 18) all have very low TOC contents (Table 1), show high degrees of bioturbation and destruction of primary fabrics, and by comparison to the carbonaceous mudstone FA's appear to have been deposited under oxygenated and likely shallower conditions. They are dominated by clastic sand to silt-sized dolomite grains that have suffered variable degrees of recrystallization (Fig. 19E). Even though primary sedimentary structures are rarely preserved, the grain size strongly suggests deposition by currents that moved sand-silt size particles as bedload. The dolarenite facies association (DA), filling in channels that have been eroded into the underlying Middle Portwood (Figs. 2 and 3) probably represents very shallow water, possibly approximating in depth the thickness of incised beds (less than a meter). The two occurrences of dolarenite lags (DAL), on account of their coarse grain size, basal scouring, and wide range of component particles, suggest substantial winnowing and stratigraphic condensation, and may record multiple episodes of storm wave impingement at surfaces with exceedingly small net sedimentation. The coarse dolosiltite (DS) FA also occurs in stratigraphic positions (Fig. 3) that suggest abundant winnowing and good oxygenation (fabric disruption), possibly as the culmination of parasequence buildup into shallower water. Better preservation of relict primary fabrics (Fig. 19D) in clayey dolosiltite (FA CDS) suggest that this dolomitic FA, relative to FA DS, was deposited in slightly deeper water with somewhat lower oxygen levels.

6.3. Redox conditions

Vertical changes of bioturbation intensity in the Portwood Member (Fig. 3; Table 1) suggests variable and frequently shifting benthic oxygen levels. The presence of glauconite grains throughout the succession suggest the former presence of benthic fecal pellets (Odin, 1988), and the need for mildly reducing pore waters during glauconite formation suggests suboxic conditions as a beneficial environmental variable (Hiscott, 1982; Odin, 1988).

Macroscopically visible bioturbation, as shown by BI (Table 1) is highly variable stratigraphically (Fig. 3), and indicates a wide range of bottom water oxygenation during deposition of the Portwood Member. Ubiquitous cryptobioturbation and compositional banding (lack of sharp layer boundaries) suggests a "background" meiofaunal activity in surficial muds. In modern oxygen limited muddy environments, sub-mm organisms (benthic agglutinated foraminifera, nematodes, and polychaetes, etc.) inhabit the uppermost millimeters to centimeters of the very water-rich surface muds (Pike et al., 2001; Bernhard et al., 2003). These organisms are all metazoans, require at least some oxygen (Bernhard et al., 2003), and suggest at a minimum suboxic conditions (Schieber, 2009, 2012). While moving through the substrate they tend to displace particles and diminish original layer to layer contrast, rather than producing significant fabric disruption and readily visible burrows that would be captured by BI (Schieber, 2014). The common observation of agglutinated benthic foraminifera in Portwood thin sections adds support to the assumption of rather pervasive benthic colonization of Portwood strata and suggests suboxic rather than anoxic as the lowest level of bottom water oxygenation (Schieber, 2009, 2012).

The completely bioturbated dolomite-rich facies associations (FA's DA, DAL, DS, and CDS; Fig. 18) indicate a well-aerated environment that enabled substrate colonization by a diverse macrofauna assembly of burrowers and sediment swimmers. The "megaburrow bed" (Brett et al., 2018) at the base of the middle Portwood (FA DA, Figs. 2 and 3) implies activity of large crustaceans, and provides further evidence for a well-aerated setting for FA's DA and DS. The almost complete obliteration of primary stratification in FA's DA and DS suggests deposition in a more stable sub-wave base setting, although the presence of scattered ooids (Fig. 19) suggests deposition adjacent to above wave base environments.

Bottom water oxygenation during deposition of the SM FA was likely

in the dysoxic to oxic range, as suggested by bioturbation intensities (Table 1). Common soft to firm-ground burrows indicate oxygen availability in bottom waters (Figs. 12 and 14) that were in excess of the suboxic background oxygenation suggested by benthic agglutinated foraminifera (see above). Graded silt to sand layers with scoured bases (Figs. 12 and 14) are generally more visibly bioturbated than under and overlying layers. Assuming a storm origin for these layers may indicate intermittent "oxygenation spikes" due to mixing of the water column by storm waves, creating temporary improvement of living conditions for benthic fauna (Föllmi and Grimm, 1990).

In the laminated FA's (LDM, LM) the macroscopically visible bioturbation, as quantified by BI (Table 1), is lowest and suggests a lesser degree of bottom water oxygenation relative to other FA's. Subtle fabric disruption by meiofauna, however, as suggested by cryptobioturbation and compositional banding (Figs. 16 and 17) is of comparable magnitude as seen in other FA's. Given the added presence of benthic agglutinated foraminifera this suggests prevalent suboxic bottom water oxygenation (Pike et al., 2001; Bernhard et al., 2003; Schieber, 2009; Löhr and Kennedy, 2015) with intermittent improvement to dysoxic conditions.

Centimeter to decimeter scale interbedding of LM and GM FA's during Upper Portwood deposition (Fig. 2) indicates cyclic improvements of bottom water oxygen availability from suboxic (LM) to dysoxic (GM). The presence of marcasitic lags in FA GM also suggests improved oxygen penetration of the substrate during GM deposition (Schieber, 2011b). Potential causes of the cyclic alternation of LM and GM are discussed in the section on sequence stratigraphic implications.

6.4. Organic matter enrichment

An increase in terrestrial siliciclastic flux (dilution) is generally considered to be associated with decreasing organic carbon content (Tyson, 1995; Liu et al., 2019b). However, siliciclastic input is not the major controlling factor for organic carbon dilution in the Portwood Member. It is quite obvious in Fig. 3 that TOC content correlates negatively with carbonate mineral content. In prior studies of OM-rich Devonian shales in the Appalachian Basin, their low carbonate content was interpreted as a consequence of acidic pore waters associated with anoxia and redox processes (Reaves, 1986; Ver Straeten et al., 2011). This explanation, however, does not fit the Portwood Member which appears to have been deposited under oxygen-bearing waters and shows well-preserved clastic carbonate grains (Fig. 4). It appears more plausible that influx of detrital carbonate represents the main dilution effect on OM enrichment in Portwood mudstones, and that dilution by siliciclastic sediments from the Acadian Orogen is negligible in comparison.

Tasmanites cysts are composed mainly of complex lipid-like substances and are highly resistant to chemical breakdown and bacterial degradation (Tappan, 1980), when compared to AOM (Liu et al., 2019b, 2020). TOM was likely sourced from the Acadian Orogen and delivered to the Portwood mudstone along with siliciclastic materials. Neither *Tasmanites* or TOM require anoxic conditions to be preserved. In combination with sedimentary features that attest to bottom currents, storm reworking, and benthic life, all available observations suggest that bottom water anoxia and a quiet environment were not needed for OM enrichment in Portwood mudstones.

The lack of AOM in the matrix and relative abundance of *Tasmanites* cysts in the GM FA (Fig. 17B) can be attributed to a combination of low sedimentation rate and increased oxygen availability. During episodes of sediment starvation, for example at marine flooding surfaces, OM in surface sediments experiences enhanced surficial microbial degradation (Ibach, 1982; Bohacs et al., 2005; Liu et al., 2019b). Whereas AOM is prone to be remineralized and destroyed by microbial processing, the cross-linked lipid walls of *Tasmanites* cysts resist microbial degradation and have high preservation potential, resulting in the observed OM distribution in FA GM. In addition, the concentration of storm-induced winnowing at flooding surfaces further enhances oxidation as well as

mechanical removal of OM (Schieber, 1998; Bohacs et al., 2005).

6.5. The sequence stratigraphic dimension - understanding portwood carbonate distribution as a consequence of sea level change

We consider the tripartite subdivision of the Portwood by Brett et al. (2018) and its correlation with the Tully interval of New York as significant progress to understand the origin of this complex stratigraphic interval. Having said this, it is equally apparent from their paper that the carbonate-rich intervals received most of the attention during their investigation. The mudstone-dominated intervals that constitute approximately 80% of the succession were not examined as closely, continuing a tradition wherein shales and mudstones are viewed as the “spacers” between more interesting lithologies of greater intellectual interest (Potter et al., 1980). That state of affairs is owed to the fact that the study of Brett et al. (2018) did not include thin section based assessment of mudstone microfacies, and reached its conclusions largely on the basis of outcrop observations, with a focus on establishing the temporal relationship of these rocks to the Tully Limestone in New York.

6.5.1. Lower Portwood

Aiming to fill this gap in perception, our investigation clearly shows that there is a level of compositional and textural detail within Portwood mudstones that allows for a much more differentiated appreciation of this succession with regard to stratigraphic evolution and changing depositional setting through time (Figs. 2 and 3). Working through the section from bottom to top, the basal 30 cm's that constitute the Lower Portwood start with a transgressive lag (Fig. 3) that overlies the unconformity atop the Boyle Member. Although this part of the section is not differentiated into system tracts in Fig. 3, one can view this lag deposit as the transgressive systems tract (TST) of the Lower Portwood sequence, and the overlying mudstone to dolarenite cycles as possible parasequences of the Lower Portwood highstand systems tract (HST). Given the highly variable character of the Lower Portwood between outcrops (Brett et al., 2004, 2018), however, one should probably refrain from over-interpreting the bits and pieces that remain of the Lower Portwood. What the rocks do tell us is that weathered carbonate-dominated debris was washed into a shallow sea from exposed areas in the west (Cincinnati Arch) and likely also from uplifted island-forming blocks along the western edge of the Appalachian Basin. The latter likelihood is supported by observations that suggest that the top of the Boyle likely was a karstified unconformity with as much as 10 m of local relief (Brett et al., 2018). Given the preponderance of sand- to mud-sized detrital carbonate grains above the basal lag, and the observation of cross-lamination in dolarenite beds, the sea must have been rather shallow so that storm-driven currents were able to transport that material offshore.

6.5.2. Middle Portwood

The Middle Portwood commences with a thick dolarenite bed that carries large crustacean burrows at the base (Fig. 3). These burrows were emplaced into a comparatively firm, but unlithified mudstone beneath the presumed sequence boundary (Brett et al., 2004, 2018), suggesting that there is only a small gap in time between the Lower and Middle Portwood. Given that the basal bed consists largely of detrital dolomite grains, it is an extrabasinal sandstone found directly above a sequence boundary (Brett et al., 2018) and can therefore be considered a basal lowstand systems tract (LST) deposit. Not recognizing its clastic character, would of course lead to its interpretation as a transgressive systems tract (TST) instead (Brett et al., 2018). The next 2 m consist of alternating packages of LDM and SM FA's. Given the more energetic and likely shallower setting of the SM FA (when compared to the LDM FA), the observed LDM-SM stacking can be interpreted as upward shallowing parasequences (Fig. 3), and the upwards decreasing thickness of the SM packages probably indicates an upwards increase of water depth. It thus appears sensible to place a transgressive surface (TS) at the top of the

basal dolarenite bed (at 0.57 m; Fig. 3) and consider the overlying interval a TST. That the tops of the SM packages are indeed marine flooding surfaces is supported by indications of very slow sedimentation and hiatus formation, such as lag development and pyrite concretions below these surfaces (Fig. 3).

A condensed interval between 2.3 and 2.5 m (Fig. 3) is marked by reworked dolosiltite beds (DS FA) with basal scours, abundant glauconite and high abundance of diagenetic overgrowth on detrital dolomite grains (e.g. Fig. 4A and B). We placed a maximum flooding surface (MFS) at the top of the upper DS bed (at 2.44 m), on account of its high glauconite contents (Fig. 3) and associated pyrite nodules beneath.

The sharp-based black-gray cycles (Figs. 2D and 15) that make up the remainder of the Middle Portwood (2.5–3.4 m; Fig. 3) represent by this logic the HST. As already discussed in section 7.2 above, these cycles can be considered shallowing upwards parasequences that originated when parasequences built upwards from “deeper” and poorly aerated conditions to shallower conditions with better oxygen supply in comparatively shallow water (Spencer, 2013). Cycles of this character are a common element of shallow water (10's of meters, Schieber, 1994) Devonian shale successions elsewhere, for example in the Selmier and Camp Run Members of the New Albany Shale in the Illinois Basin (Schieber and Lazar, 2004; Lazar, 2007), and the Upper Dowelltown Member of the Chattanooga Shale (Schieber, 1994, 1998; Lobza and Schieber, 1999). Although some may consider these cycles to be too “thin” to be considered parasequences, one needs to consider that the study area is rather distal relative to the shoreline (ca. 300 km to the east), was severely starved of terrigenous input (Smith et al., 2019), and consequently represents a condensed section. The Middle Portwood terminates (at 3.4 m) against an erosion surface that carved channel-like incisions of as much as half a meter local relief into the underlying Middle Portwood succession (Fig. 2E). This surface is considered the second sequence boundary within the Portwood succession (Brett et al., 2018), and marks a significant drop of relative sea level.

6.5.3. Upper Portwood

As the preceding sequence, the Upper Portwood starts with a dolomite bed that fills pre-existing topography (Fig. 2). Careful examination shows that it actually consists of sand-size detrital dolomite (Fig. 19E). Therefore it is best considered a lowstand deposit (LST), rather than an expression of minimal terrigenous sedimentation related to transgression (Fig. 3). Overlying beds of the CDS FA are separated by softer weathering thin GM intervals (Figs. 2 and 3). The latter are considered the basal portions of shallowing upwards GM-CDS parasequences. The lateral continuity of these parasequences across the outcrop contrasts with the underlying dolarenite (DA) lowstand deposit, and suggests more uniform sediment dispersal and increasing water depth. Consequently, a TS is placed at the contact between the lenticular DA bed and the overlying CDS FA (Fig. 3), and the interval from 3.8 to 4.22. m is interpreted as a TST.

A condensed interval between 4.42 and 4.63 m (Fig. 3) is marked by a prominent (Fig. 2E) highly OM-enriched black shale bed (LM FA). To be consistent with the interpretation of the underlying Middle Portwood, the MFS was placed at the top of the glauconite-enriched dolosiltite bed (at 4.6 m) within this interval.

The succession above the MFS is characterized by multiple sharp-based black-gray cycles, and marks a “turn around” of the depositional system similar to that seen near the top of the Middle Portwood. As in the HST of the Middle Portwood (see above), these cycles are interpreted as parasequences (Fig. 3), their thin nature attributable to distal setting and sediment starvation. The observation that these cycles contain less detrital dolomite than underlying mudstones (Table 1) may indicate that the supply of detrital dolomite is dwindling because most of the earlier “high” spots (islands) have finally been flooded. The observation that the well-rounded quartz grains that were common in the Lower and Middle Portwood (Fig. 3) are no longer observed in the Upper Portwood supports this assumption, because it implies that exposures (to the west)

that supplied these grains have finally been submerged. The implication of this reasoning is a generally greater water depth for the HST of the Upper Portwood, relative to the HST of the Middle Portwood. Yet, the lighter gray color of the upper half of the Upper Portwood black-gray cycles (Figs. 2E and 16) nonetheless implies improved (and deeper) oxygenation of the water column, possibly a consequence of better circulation in a somewhat deeper sea with fewer obstacles (drowned islands) to large-scale circulation cells.

Along outcrop truncation of Upper Portwood black-gray cycles beneath the Trousdale Member of the New Albany Shale indicate the presence of another significant erosion surface of sequence boundary rank. This inference is supported by the observed abrupt change from interbedded back-gray to solid black shale (Fig. 2). At a minimum it implies a relative lowering of sea level that allowed waves and currents to effectively erode parts of the Upper Portwood succession.

7. Summary and conclusions

In the carbonate-rich Portwood succession, detrital dolomite in essence took the place of what “normally” would have been detrital quartz. Recognizing the dolomite as clastic input, rather than as a “locally grown” carbonate sediment or cement profoundly impacts the appropriate sequence stratigraphic interpretation of the succession. Strata that traditionally would have been interpreted as associated with rising sea level and flooding (TST), need instead be understood as sand-rich lowstand (LST) deposits. The ensuing shift of perspective also necessitates fundamentally different placement of transgressive (TS) and maximum flooding (MFS) surfaces, as well as system tracts. Although detrital carbonate can mask and obscure the diagenetic carbonate signatures in mudstone successions that we associate with low sedimentation rates and sediment starvation, detailed outcrop (or core) description and petrography can discover and identify condensed horizons and flooding surfaces, for example via presence of glauconite, pyrite nodules, and abundant carbonate cement between detrital dolomite grains. The Portwood succession serves as an excellent example on how even thin mudstone successions can through careful petrographic analysis be subdivided into sequences, system tracts, and even para-sequences, and be subject to sophisticated sequence stratigraphic analysis.

Declaration of competing interest

The authors declare that they have no known competing financial interests or personal relationships that could have appeared to influence the work reported in this paper.

Acknowledgements

This research was supported by the sponsors of the Indiana University Shale Research Consortium (Anadarko, Chevron, ConocoPhillips, ExxonMobil, Shell, Statoil, Marathon, Whiting Oil and Wintershall). Financial support for Xinhe Shao from the China Scholarship Council and an AAPG Foundation Grant-in-Aid Award is gratefully acknowledged. An NSF equipment grant to Juergen Schieber (EAR-0318769) provided funds for the purchase of the analytical SEM that was used to acquire SEM images used in this report.

References

Aigner, T., Reineck, H.E., 1982. Proximity trends in modern storm sands from the Helgoland Bight (North Sea) and their implications for basin analysis. *Senckenberg. Maritima* 14, 183–215.

Allen, J.R.L., 1985. *Principles of Physical Sedimentology*. Chapman & Hall, London, p. 272.

Amsbury, D.L., 1962. Detrital dolomite in central Texas. *J. Sediment. Res.* 32, 5–14.

Baird, G.C., Brett, C.E., 2008. Late givetian taghanic bioevents in New York state: new discoveries and questions. *Bull. Geosci.* 83, 357–375.

Baker, P.A., Kastner, M., 1981. Constraints on the formation of sedimentary dolomite. *Science* 213, 214–216.

Barnett, S.F., Ettensohn, F.R., Mellon, C., 1989. Tectonic and flexural significance of middle Devonian graben-fill sequence in new Albany shale, central Kentucky. In: AAPG Eastern Section Meeting, Bloomington, IN, USA, September 10–13, 1989. AAPG Search and Discovery. Article 91023.

Barnett, S.F., Ettensohn, F.R., 1992. Portwood member of the new Albany shale and the Boyle dolostone. In: Ettensohn, F.R. (Ed.), *Changing Interpretations of Kentucky Geology: Layer-Cake, Facies, Flexure, and Eustasy*. Ohio Division of Geological Survey, Miscellaneous Report 5, pp. 42–44.

Barnett, S.F., Ettensohn, F.R., 2003. A possible middle Devonian tsunamite: Duffin bed, new Albany shale of south-central Kentucky. *GSA Abstracts with Programs* 35, 602.

Basu, A., Schieber, J., Patranabis-Deb, S., Dhang, P.C., 2013. Recycled detrital quartz grains are sedimentary rock fragments indicating unconformities: examples from the Chhattisgarh Supergroup, Bastar Craton, India. *J. Sediment. Res.* 83, 368–376.

Bernhard, J.M., Visscher, P.T., Bowser, S.S., 2003. Sub-millimeter life positions of bacteria, protists, and metazoans in laminated sediments of the Santa Barbara Basin. *Limnol. Oceanogr.* 48, 813–828.

Bohacs, K.M., Grabowski Jr., G.J., Carroll, A.R., Mankiewicz, P.J., Miskell-Gerhardt, K.J., Schwalbach, J.R., Wegner, M.B., Simo, J.A., 2005. Production, destruction, and dilution—the many paths to source-rock development. In: Harris, N.B. (Ed.), *The Deposition of Organic-Carbon Rich Sediments: Models, Mechanisms, and Consequences*, vol. 82. SEPM Special Publication, pp. 61–101.

Brett, C.E., 1995. Sequence stratigraphy, biostratigraphy, and taphonomy in shallow marine environments. *Palaios* 10, 597–616.

Brett, C.E., Baird, G.C., Bartholomew, A.J., 2004. Sequence stratigraphy of highly variable Middle Devonian strata in central Kentucky: implications for regional correlations and depositional environments. In: Schieber, J., Lazar, R.O. (Eds.), *Devonian Black Shales of the Eastern U.S.: New Insights into Sedimentology and Stratigraphy from the Subsurface and Outcrops in the Illinois and Appalachian Basins*. Field Guide for the 2004 Annual Field Conference of the Great Lakes Section of SEPM, Indiana Geological Survey Open File Study, 04–05, pp. 35–60.

Brett, C.E., Allison, P.A., Hendy, A.J.W., 2011. Comparative taphonomy and sedimentology of small-scale mixed carbonate/siliciclastic cycles: synopsis of Phanerozoic examples. In: Allison, P.A., Bottjer, D.J. (Eds.), *Taphonomy: Process and Bias through Time*, second ed. Springer, Dordrecht Heidelberg, London, New York, pp. 107–199.

Brett, C.E., Zambito, J.J., Baird, G.C., Aboussalam, Z.S., Becker, R.T., Bartholomew, A.J., 2018. Litho-, bio-, and sequence stratigraphy of the Boyle-Portwood succession (middle Devonian, central Kentucky, USA). *Palaeobiodivers. Palaeoenviron.* 98, 331–368.

Camp, W.K., Egenhoff, S., Schieber, J., Slatt, R.M., 2016. A compositional classification for grain assemblages in fine-grained sediments and sedimentary rocks-discussion. *J. Sediment. Res.* 86, 1–5.

Campbell, G., 1946. New Albany shale. *GSA Bulletin* 57, 829–908.

Cocks, L.R.M., Torsvik, T.H., 2002. Earth geography from 500 to 400 million years ago: a faunal and paleomagnetic review. *J. Geol. Soc.* 159, 631–644.

Compton, J.S., 1988. Degree of supersaturation and precipitation of organogenic dolomite. *Geology* 16, 318–321.

Cuomo, M.C., Bartholomew, P.R., 1991. Pelletal black shale fabrics: their origin and significance. In: Tyson, R.V., Pearson, T.H. (Eds.), *Modern and Ancient Continental Shelf Anoxia*, vol. 58. Geological Society of London, Special Publication, pp. 221–232.

Dolan, J.F., 1989. Eustatic and tectonic controls on deposition of hybrid siliciclastic/carbonate basinal cycles: discussion with examples. *AAPG (Am. Assoc. Pet. Geol.) Bull.* 73, 1233–1246.

Dott, R.H., 2003. The importance of eolian erosion in supermature quartz sandstones and the paradox of weathering on vegetation-free landscapes. *J. Geol.* 111, 387–405.

Ettensohn, F.R., 1985. The Catskill delta complex and the Acadian orogeny: a model. In: Woodrow, D.L., Sevon, W.D. (Eds.), *The Catskill Delta*. GSA Special Paper 201, pp. 39–50.

Ettensohn, F.R., 1987. Rates of relative plate motion during the Acadian Orogeny based on the spatial distribution of black shales. *J. Geol.* 95, 572–582.

Ettensohn, F.R., Miller, M.L., Dillman, S.B., Elam, T.D., Geller, K.L., Swager, D.R., Markowitz, G., Woock, R.D., Barron, L.S., 1988. Characterization and implications of the Devonian-Mississippian black shale sequence, eastern and central Kentucky, USA: Pycnoclines, transgression, regression, and tectonism. In: McMillan, N.J., Embry, A.F., Glass, D.J. (Eds.), *Devonian of the World, Vol. II: Sedimentation*, vol. 14. Canadian Society of Petroleum Geologists Memoir, pp. 323–346.

Ettensohn, F.R., 1994. Tectonic control on formation cyclicity of major Appalachian unconformities and associated stratigraphic sequences. In: Dennison, J.M., Ettensohn, F.R. (Eds.), *Tectonic and Eustatic Controls on Sedimentary Cycles*, SEPM Concepts in Sedimentology and Paleontology, vol. 4, pp. 217–242.

Ettensohn, F.R., 2008. The Appalachian foreland basin in eastern United States. In: Miall, A.D. (Ed.), *The Sedimentary Basins of the United States and Canada*. Elsevier, Amsterdam, pp. 105–179.

Flügel, E., 2004. *Microfacies of Carbonate Rocks: Analysis, Interpretation and Application*. Springer-Verlag, Berlin, p. 976.

Folk, R.L., 1980. *Petrology of Sedimentary Rocks*. Hemphill Publishing, Austin, p. 182.

Föllmi, K.B., Grimm, K.A., 1990. Doomed pioneers: gravity-flow deposition and bioturbation in marine oxygen-deficient environments. *Geology* 18, 1069–1072.

Ghadeer, S.G., Macquaker, J.H., 2011. Sediment transport processes in an ancient mud-dominated succession: a comparison of processes operating in marine offshore settings and anoxic basinal environments. *J. Geol. Soc.* 168, 1121–1132.

Garrels, R.M., Thompson, M.E., Siever, R., 1960. Stability of some carbonates at 25 degrees C and one atmosphere total pressure. *Am. J. Sci.* 258, 402–418.

- Gray, H.H., Ault, C.H., Keller, S.J., 1987. Bedrock geologic map of Indiana. Indiana Geol. Surv. Misc. Map 48 scale 1:500,000.
- Hiscott, R.N., 1982. Tidal deposits of the lower Cambrian random formation, eastern Newfoundland: facies and paleoenvironments. *Can. J. Earth Sci.* 19, 2028–2042.
- Holland, S.M., 1993. Sequence stratigraphy of a carbonate-clastic ramp: the Cincinnati Series (Upper Ordovician) in its type area. *GSA Bulletin* 105, 306–322.
- Ibach, L.E.J., 1982. Relationship between sedimentation rate and total organic carbon content in ancient marine sediments. *AAPG (Am. Assoc. Pet. Geol.) Bull.* 66, 170–188.
- Jordan, D.W., 1985. Trace fossils and depositional environments of Upper Devonian black shales, east-central Kentucky, U.S.A. In: Curran, H.A. (Ed.), *Biogenic Structures: Their Use in Interpreting Depositional Environments*, vol. 35. SEPM Special Publication, pp. 279–298.
- Johnson, J.G., 1970. Taghanic onlap and the end of North America Devonian provinciality. *GSA Bulletin* 81, 2077–2105.
- Kastner, M., Elderfield, H., Martin, J.B., Suess, E., Kvenvolden, K.A., Garrison, R.E., 1990. Diagenesis and interstitial-water chemistry at the Peruvian continental margin—major constituents and strontium isotopes. In: Suess, E., von Huene, R., et al. (Eds.), *Proceedings of the Ocean Drilling Program, Scientific Results*, vol. 112, pp. 413–440.
- Kepferle, R.C., Roen, J.B., 1981. Chattanooga and Ohio shales of the southern Appalachian basin. In: Roberts, T.G. (Ed.), *GSA Cincinnati '81 Field Trip Guidebooks*, Vol. II: Economic Geology, Structure. American Geological Institute, pp. 259–323.
- Kjørboe, T., 2000. Colonization of marine snow aggregates by invertebrate zooplankton: abundance, scaling, and possible role. *Limnol. Oceanogr.* 45, 479–484.
- Kuenen, P.H., 1960. Experimental abrasion 4: Eolian action. *J. Geol.* 68, 427–449.
- Langmuir, D., 1997. *Aqueous Environmental Chemistry*. Prentice Hall, New York, p. 600.
- Lazar, O.R., 2007. Redefinition of the New Albany Shale of the Illinois Basin: an Integrated, Stratigraphic, Sedimentologic, and Geochemical Study (Ph.D. dissertation). Indiana University, Bloomington, p. 336.
- Lazar, O.R., Bohacs, K.M., Macquaker, J.H., Schieber, J., Demko, T.M., 2015a. Capturing key attributes of fine-grained sedimentary rocks in outcrops, cores, and thin sections: Nomenclature and description guidelines. *J. Sediment. Res.* 85, 230–246.
- Lazar, R., Bohacs, K.M., Schieber, J., Macquaker, J., Demko, T., 2015b. Mudstone Primer: Lithofacies variations, diagnostic criteria, and sedimentologic/stratigraphic implications at the lamina to bedset scale. *SEPM Concepts Sedimentol. Paleontol.* #12, 198.
- Li, Z., Schieber, J., 2018. Composite particles in mudstones: examples from the late cretaceous Tununk shale member of the Mancos shale formation. *J. Sediment. Res.* 88, 1319–1344.
- Li, Z., Schieber, J., 2020. Application of sequence stratigraphic concepts to the Upper Cretaceous Tununk Shale Member of the Mancos Shale Formation, south-central Utah: Parasequence styles in shelfal mudstone strata. *Sedimentology* 67, 118–151.
- Li, Z., Schieber, J., Pedersen, P.K., 2020. On the origin and significance of composite particles in mudstones: Examples from the Cenomanian Dunvegan Formation. *Sedimentology*. <https://doi.org/10.1111/sed.12801>.
- Lindholm, R.C., 1969. Detrital dolomite in Onondaga limestone (Middle Devonian) of New York: its implications to the “Dolomite question”. *AAPG (Am. Assoc. Pet. Geol.) Bull.* 53, 1035–1042.
- Liu, B., Schieber, J., Mastalerz, M., 2017. Combined SEM and reflected light petrography of organic matter in the New Albany Shale (Devonian-Mississippian) in the Illinois Basin: A perspective on organic pore development with thermal maturation. *Int. J. Coal Geol.* 184, 57–72.
- Liu, B., Schieber, J., Mastalerz, M., 2019a. Petrographic and micro-FTIR study of organic matter in the Upper Devonian New Albany Shale during thermal maturation: Implications for kerogen transformation. In: Camp, W., Milliken, K., Taylor, K., Fishman, N., Hackley, P., Macquaker, J. (Eds.), *Mudstone Diagenesis: Research Perspectives for Shale Hydrocarbon Reservoirs, Seals, and Source Rocks*, vol. 120. AAPG Memoir, pp. 165–188.
- Liu, B., Schieber, J., Mastalerz, M., Teng, J., 2019b. Organic matter content and type variation in the sequence stratigraphic context of the Upper Devonian New Albany Shale, Illinois Basin. *Sediment. Geol.* 383, 101–120.
- Liu, B., Mastalerz, M., Schieber, J., Teng, J., 2020. Association of uranium with macerals in marine black shales: Insights from the Upper Devonian New Albany Shale, Illinois Basin. *Int. J. Coal Geol.* 217, 103351.
- Lobza, V., Schieber, J., 1999. Biogenic sedimentary structures produced by worms in soupy, soft muds: observations from the Chattanooga Shale (Upper Devonian) and experiments. *J. Sediment. Res.* 69, 1041–1049.
- Löhr, S.C., Kennedy, M.J., 2015. Micro-trace fossils reveal pervasive reworking of Pliocene sapropels by low-oxygen-adapted benthic meiofauna. *Nat. Commun.* 6, 1–8.
- Macquaker, J.H., Keller, M.A., Davies, S.J., 2010. Algal blooms and “marine snow”: Mechanisms that enhance preservation of organic carbon in ancient fine-grained sediments. *J. Sediment. Res.* 80, 934–942.
- Martire, L., Bertok, C., D’atri, A., Perotti, E., Piana, F., 2014. Selective dolomitization by syntaxial overgrowth around detrital dolomite nuclei: a case from the Jurassic of the Ligurian Briançonnais (Ligurian Alps). *J. Sediment. Res.* 84, 40–50.
- Mazullo, J., Ehrlich, R., 1983. Grain shape variation in the St. Peter Sandstone: a record of eolian and fluvial sedimentation of an Early Paleozoic cratonic sheet sand. *J. Sediment. Petrol.* 53, 105–119.
- Milliken, K.L., Land, L.S., 1993. The origin and fate of silt sized carbonate in subsurface Miocene-Oligocene mudstones, south Texas Gulf Coast. *Sedimentology* 40, 107–124.
- Milliken, K., Choh, S.J., Papazis, P., Schieber, J., 2007. “Cherty” stringers in the Barnett Shale are agglutinated foraminifera. *Sediment. Geol.* 198, 221–232.
- Milliken, K., 2014. A compositional classification for grain assemblages in fine-grained sediments and sedimentary rocks. *J. Sediment. Res.* 84, 1185–1199.
- Odin, G.S., 1988. *Developments in Sedimentology*. Green Marine Clays: Oolitic Ironstone Facies, Verdine Facies, Glaucony Facies and Celadonite-Bearing Facies-A Comparative Study, vol. 45. Elsevier, p. 445.
- Pettijohn, F.J., Potter, P.E., Siever, R., 1987. *Sand and Sandstone*. Springer, New York, pp. 1–23.
- Pike, J., Bernhard, J.M., Moreton, S.G., Butler, I.B., 2001. Microbioirrigation of marine sediments in dysoxic environments: implications for early sediment fabric formation and diagenetic processes. *Geology* 29, 923–926.
- Potter, P.E., Maynard, J.B., Pryor, W.A., 1980. *Sedimentology of Shale: Study Guide and Reference Sources*. Springer-Verlag, New York, p. 303.
- Reaves, C.M., 1986. Organic matter metabolizability and calcium carbonate dissolution in nearshore marine muds. *J. Sediment. Res.* 56, 486–494.
- Riese, D., 2014. The Significance of Crypto-And Macrobioirrigation in the New Albany Shale for the Interpretation of Depositional Histories: an Integrated Approach Using Core Descriptions, CT Scans, Neochronology Experiments, and Geochemistry (Ph.D. dissertation). Indiana University, Bloomington, p. 301.
- Savage, T.E., 1930. Devonian rocks of Kentucky. *Kentucky Geol. Surv., series 6* 33, 1–161.
- Schieber, J., 1990. Significance of styles of epicontinental shale sedimentation in the Belt Basin, Mid-Proterozoic of Montana, USA. *Sediment. Geol.* 69, 297–312.
- Schieber, J., 1994. Evidence for high-energy events and shallow-water deposition in the Chattanooga Shale, Devonian, central Tennessee, USA. *Sediment. Geol.* 93, 193–208.
- Schieber, J., 1998. Sedimentary features indicating erosion, condensation, and hiatuses in the Chattanooga Shale of Central Tennessee: relevance for sedimentary and stratigraphic evolution. In: Schieber, J., Zimmer, W., Sethi, P.S. (Eds.), *Shales and Mudstones*, Vol. I: Basin Studies, Sedimentology and Paleontology. Schweizerbart'sche, Stuttgart, pp. 187–215.
- Schieber, J., 1999. Distribution and deposition of mudstone facies in the Upper Devonian Sonyea Group of New York. *J. Sediment. Res.* 69, 909–925.
- Schieber, J., 2003. Depositional Fabric of Mudstones. In: Middleton, G.V. (Ed.), *Encyclopedia of Sediments and Sedimentary Rocks*. Kluwer Scientific Publishers, Dordrecht, pp. 203–207.
- Schieber, J., Baird, G., 2001. On the origin and significance of pyrite spheres in Devonian black shales of North America. *J. Sediment. Research* 71 (1), 155–166.
- Schieber, J., Lazar, R.O., 2004. Devonian Black Shales of the Eastern U.S.: New Insights into Sedimentology and Stratigraphy from the Subsurface and Outcrops in the Illinois and Appalachian Basins. *Field Guide for the 2004 Annual Field Conference of the Great Lakes Section of SEPM*. No. 5, 4. Indiana Geological Survey Open File Study 04–05, p. 90.
- Schieber, J., Southard, J., Thaisen, K., 2007. Accretion of mudstone beds from migrating floccule ripples. *Science* 318, 1760–1763.
- Schieber, J., 2009. Discovery of agglutinated benthic foraminifera in Devonian black shales and their relevance for the redox state of ancient seas. *Palaeogeogr. Palaeoclimatol. Palaeoecol.* 271, 292–300.
- Schieber, J., 2011a. Reverse engineering mother nature-shale sedimentology from an experimental perspective. *Sediment. Geol.* 238, 1–22.
- Schieber, J., 2011b. Marcasite in black shales—a mineral proxy for oxygenated bottom waters and intermittent oxidation of carbonaceous muds. *J. Sediment. Res.* 81, 447–458.
- Schieber, J., 2012. Styles of agglutination in benthic foraminifera from modern Santa Barbara Basin sediments and fossil analogs in Devonian and Mississippian black shales. In: Altenbach, A.V., Bernhard, J.M., Seckbach, J. (Eds.), *Anoxia: Evidence for Eukaryote Survival and Paleontological Strategies*. Springer, New York, pp. 575–589.
- Schieber, J., 2014. Traces in the dark—Sedimentary processes and facies gradients in the Upper Devonian–Lower Mississippian Upper Shale Member of the Bakken Formation, Williston Basin, North Dakota, U.S.A.—Discussion. *J. Sediment. Res.* 84, 837–838.
- Schieber, J., 2016a. Experimental testing of the transport-durability of shale lithics and its implications for interpreting the rock record. *Sediment. Geol.* 331, 162–169.
- Schieber, J., 2016b. Mud re-distribution in epicontinental basins—Exploring likely processes. *Mar. Petrol. Geol.* 71, 119–133.
- Scotese, C.R., McKerrrow, W.S., 1990. Revised world maps and introduction. In: McKerrrow, W.S., Scotese, C.R. (Eds.), *Paleozoic Paleogeography and Biogeography*. The Geological Society (London) Memoir 12, pp. 1–21.
- Scotese, C.R., 2001. *Atlas of Earth History*, vol. 1. Paleogeography, PALEOMAP Project, University of Texas, Arlington, p. 52. <http://www.scotese.com/>.
- Scotese, C.R., 2009. Paleogeographic Map Archive, PALEOMAP Project. University of Texas, Arlington, p. 52. <http://www.scotese.com/>.
- Smith, L.B., Schieber, J., Wilson, R.D., 2019. Shallow-water onlap model for the deposition of Devonian black shales in New York, USA. *Geology* 47, 279–283.
- Spencer, S.C., 2013. An Investigation of Parasequences in the Camp Run Member of the Upper Devonian New Albany Shale. AAPG Search and Discovery Article #50891.
- Tappan, H., 1980. The Paleobiology of Plant Protists. Freeman, San Francisco, p. 1028.
- Taylor, K.G., Gawthorpe, R.L., Curtis, C.D., Marshall, J.D., Awwiller, D.N., 2000. Carbonate cementation in a sequence-stratigraphic framework: Upper Cretaceous sandstones, Book Cliffs, Utah-Colorado. *J. Sediment. Res.* 70, 360–372.
- Taylor, K.G., Macquaker, J.H.S., Shaw, H., 2014. Diagenetic alterations in a silt- and clay-rich mudstone succession: an example from the Upper Cretaceous Mancos Shale of Utah, USA. *Clay Miner.* 49, 213–227.
- Trabucho-Alexandre, J., 2014. More gas than shale: erosion of mud and its effect on preserved geochemical and palaeobiological signals. In: Smith, D.G., Bailey, R.J., Burgess, P.M., Fraser, A.J. (Eds.), *Strata and Time: Probing the Gaps in Our Understanding*, vol. 404. Geological Society of London Special Publication, pp. 251–270.

- Tyson, R.V., 1995. *Sedimentary Organic Matter: Organic Facies and Palynofacies*. Chapman & Hall, London, p. 615.
- Van Sicken, D.C., 1958. Depositional topography—examples and theory. AAPG (Am. Assoc. Pet. Geol.) Bull. 42, 1897–1913.
- Van Wagoner, J.C., Mitchum, R.M., Campion, K.M., Rahmanian, V.D., 1990. Siliciclastic sequence stratigraphy in well logs, cores, and outcrops: concepts for high-resolution correlation of time and facies. AAPG Methods Explor. Ser. 7, 55.
- Ver Straeten, C.A., Brett, C.E., Sageman, B.B., 2011. Mudrock sequence stratigraphy: A multi-proxy (sedimentological, paleobiological and geochemical) approach, Devonian Appalachian Basin. *Palaeogeogr. Palaeoclimatol. Palaeoecol.* 304, 54–73.
- Wetzel, A., Allia, V., 2000. The significance of hiatus beds in shallow-water mudstones: an example from the Middle Jurassic of Switzerland. *J. Sediment. Res.* 70, 170–180.
- Wilson, R.D., Schieber, J., 2015. Sedimentary facies and depositional environment of the Middle Devonian Genesee Formation of New York, USA. *J. Sediment. Res.* 85, 1393–1415.
- Witzke, B.J., Heckel, P.H., 1988. Paleoclimatic indicators and inferred Devonian paleolatitudes of Euramerica. In: McMillan, N.J., Embry, A.F., Glass, D.J. (Eds.), *Devonian of the World, Vol. I: Regional Syntheses*. Canadian Society of Petroleum Geologists Memoir, pp. 49–63, 14.
- Yawar, Z., Schieber, J., 2017. On the origin of silt laminae in laminated shales. *Sediment. Geol.* 360, 22–34.
- Zuffa, G.G., 1980. Hybrid arenites: their composition and classification. *J. Sediment. Petrol.* 50, 21–29.